Preliminary studies of a regional aircraft with hydrogen-based hybrid propulsion

Vincenzo Palladino, Arnaud Jordan, Nathalie Bartoli, Peter Schmollgruber, Valérie Pommier-Budinger, Emmanuel Benard

Preliminary studies of a regional aircraft with hydrogen-based hybrid propulsion

Vincenzo Palladino* and Arnaud Jordan †
ATR Aircraft, Blagnac, France, 31712

Nathalie Bartoli‡ and Peter Schmollgruber§
ONERA/DTIS-Université de Toulouse, Toulouse, France, 31055

Valérie Pommier-Budinger¶ and Emmanuel Benard ‖
ISAE-SUPAERO, Toulouse, France, 31055

This paper addresses the topic of conceptual design of a regional aircraft with hybrid electric propulsion based on hydrogen fuel cells. It aims at proving the interest in the fuel cell technology for a regional aircraft of the 70-80 seat class to reduce its environmental impact. First, a description of the aircraft design platform used to perform the analysis is given, with a special focus on presenting the methods used to model the hydrogen-based hybrid propulsion. Then, the selection of the hybrid electric architecture and the sizing of the propulsion system are presented. Finally, the performances of the hybrid aircraft have been evaluated for different sizes of the electrical propulsive system as well as for different design missions. Comparing the results in terms of block fuel, CO_2 equivalence and NO_x emissions, with the performance of the conventional baseline aircraft, the study provides a preliminary assessment of the potential benefits to be expected by the fuel cell technology applied on a large turboprop passenger aircraft. Appreciable reductions of both CO_2 equivalence and NO_x can be observed, with peaks for the best hybrid configuration of -24% and -40%, respectively.

I. Nomenclature

SAF	=	Sustainable Aviation Fuel
$GHGs$	=	Greenhouse Gases
LHV	=	Low Heating Value
BOR	=	Boil-off rate
SFC	=	Specific Fuel Consumption
EI	=	Emission Index
$TLARs$	=	Top level Aircraft Requirements
MDA	=	Multidisciplinary Design Analysis
$RHEA$	=	Regional Hybrid Electric Aircraft
$FAST\text{-}OAD$	=	Future Aircraft Sizing Tool - Overall Aircraft Design
$MTOW$	=	Max Take-Off Weight
OWE	=	Operating Weight Empty
BF	=	Block Fuel
TTC	=	Time To Climb
TT	=	Trip Time
H_p	=	Power Hybridization Factor

*PhD candidate, Department of preliminary design and future projects, vincenzo.palladino@atr-aircraft.com
†Aerospace engineer, Department of preliminary design and future projects, arnaud.jordan@atr-aircraft.com
‡Senior researcher, Processing and Systems Department, nathalie.bartoli@onera.fr, AIAA Member MDO TC
§Program Director for Civil Transport Aircraft, peter.schmollgruber@onera.fr, AIAA Member Aircraft Design TC
¶Professor at ISAE-SUPAERO, Department of Aerospace Vehicles Design and Control, valerie.budinger@isae-supaero.fr
‖Ass. Professor at ISAE-SUPAERO, Department of Aerospace Vehicles Design and Control, emmanuel.benard@isae-supaero.fr

Subscripts

gt	=	gas turbine
pp	=	propulsion
eng	=	gas turbine and gearbox
$prop$	=	propeller
ps	=	propulsive control systems
em	=	electric motor
pe	=	power electronics
$cool$	=	cooling
fc	=	fuel cell
cmp	=	compressor
acc	=	accessories
$distr$	=	distribution
RTO	=	Reserve Take-Off

II. Introduction

One of the biggest challenges of the aviation sector, and in general of the transport sector, has been around the development of "greener" vehicles, which feature low CO_2 and NOx emissions. The European Union Commission together with aviation industry players has set the targets to be achieved by 2050 [1]: 75% CO_2 reduction, 90% NOx and 65% perceived noise reduction relatively to a reference emission scenario in the year 2000. Different technological solutions including sustainable aviation fuel (SAF), hydrogen fuel and electric propulsion, are being investigated by the main actors of the aviation sector in order to meet these ambitious targets.

The huge interest in alternative sustainable fuel is clear: it represents a drop-in solution to reduce life-cycle CO_2 emissions which only requires moderate to zero modifications to aircraft or engine design. However, there are some significant drawbacks for the use of SAF, such as the adverse side-effects arising from production of the feedstock for biofuel generation (for example, adverse impact on farming land, fresh-water supply, food prices, etc. [2]), as well as its poor cost-competitiveness and the scarce availability of resources to satisfy today and future fuel demand. For all these reason, while sustainable aviation fuel remains an interesting solution to reduce aviation related CO_2 emissions, it is clear that other technologies must be developed and implemented, together with SAF, in order to meet the ambitious aviation emission targets.

Hydrogen fuel represents a non drop-in alternative to kerosene which could lead to zero in-flight emissions of CO_2 and lower NOx emissions. The idea of burning hydrogen in a gas turbine has been around for many decades and although some studies and tests have already been performed, up to date such technology is still far from powering a commercial aircraft [3]. Electric propulsion is the most innovative, energy-efficient and climate-friendly technology which allows opening the design space to more efficient aircraft (e.g. distributed propulsion) and it can potentially reduce operational costs as well as noise emissions [4]. Electrical power can be generated in many different ways, but for on-board power generation there are mainly two alternatives: batteries or hydrogen through the use of fuel cells. Of course, electricity can also be derived by the combustion of fuel through a gas turbine generator, however it has been intentionally ruled out since potential emission reductions could only derive from an efficient air-frame design enabled by the exploitation of the electrical power and not by the electric propulsion itself.

High performance lithium-ion batteries are the most common choice in the automotive industry for both hybrid electric and full-electric vehicles. Li-ion batteries show energy and power densities which comply with the minimum operational requirements of cars and they are preferred to hydrogen fuel cells which would imply the development of hydrogen distribution networks, higher energy costs as well as higher vehicle cost due to the expensive materials used for the manufacturing of the high pressure hydrogen tanks and the fuel cells. Nevertheless, state-of-the-art battery technology shows performance and weight deficits compared to conventional aircraft propulsive systems which represent a big limit for the aviation industry. Many studies have already been performed in order to assess the actual potential of battery-based electric propulsion systems in terms of aircraft emission reductions. Whilst pure-electric configurations are not an option for regional aircraft due to the huge weight of the batteries needed to provide the necessary energy for the typical flight mission, hybrid electric configurations may be feasible with short-medium term predictions of technology levels [5, 6]. In [5], various propulsive architectures have been compared on a regional aircraft similar to

the ATR72. The study concludes that with current state-of-the-art electric components and battery technology levels (E_{sp}=200 Wh/kg for batteries) both turbo-electric and serial hybrid are responsible for a massive increase of weight and loss of total efficiency, which leads to increased fuel consumption, thus higher emissions. Only the parallel hybrid configuration shows the potential to reduce fuel consumption on a 300 NM mission. In [6], the analysis of three case studies of a 2035 turboprop regional aircraft using parallel, series/parallel and distributed series configurations also show that the improvements in terms of fuel consumption and emissions with respect to a reference ATR72 aircraft on a 800 NM mission are around 5% with a very optimistic value of battery specific energy of 500 Wh/kg at cell level. The parallel hybrid configuration is identified as the most efficient among the three architectures considered, and it is outperformed by the series/parallel and distributed series configurations only in a really optimistic scenario where batteries reach 750 Wh/kg which allows exploiting the improved aerodynamics of these configurations despite their higher weight. Similar studies on a regional turboprop ATR-like aircraft have been conducted in the past two years by [7–9]. Although the assumptions regarding components technological levels as well as top level aircraft requirements (TLARs) (e.g. mission range, speeds etc.) differ also significantly from one study to another leading to sometimes dissimilar results, a common agreement is about the conclusion that if battery technology does not improve dramatically, hybrid-electric propulsion with batteries as main electrical power source is unlikely to prove beneficial.

With the hydrogen low heating value (LHV) almost three times higher than jet fuel and an efficiency which is roughly double than gas turbines, fuel cells can be seen as key enablers for the next generation hybrid electric regional aircraft to effectively reduce emissions. A comprehensive study about hydrogen-powered aviation, procured by Clean Sky 2 JU and FCH 2 JU and financially supported under the H2020 Framework Programme, was prepared by McKinsey & Company [10]. The aforementioned document addresses technological, economical and environmental impacts of hydrogen propulsion providing a detailed assessment of its potential to reduce aviation's climate impact. By analyzing the different aircraft segments (from general aviation to long range aircraft), projecting technological developments of hydrogen combustion as well as fuel-cell powered propulsion, and considering implications on aircraft design, airport infrastructure, and hydrogen supply chains, it gives insights about the main challenges and benefits of hydrogen-powered aircraft. The study concludes that H_2 propulsion could significantly reduce climate impact (-75% to -90% with fuel-cell propulsion compared to about -30% to -60% with synfuels) and that the technological advancements needed to overcome the main technological challenges are achievable within five to ten years. In particular, the study identifies fuel cell-powered propulsion as the most energy-efficient, climate-friendly, and economic option for a regional aircraft with a capacity of 80 passengers, foreseeing CO_2 reductions up to 100% with 5% to 15% of additional costs (per seat kilometer) and a maximum take off weight increase of around 10%. However, these numbers are not the result of a detailed performance evaluation of a specific concept design, but they represent rather the potential results of the "most promising" design based on expert discussions, high-level calculations and a survey of academic literature. Despite the common belief that hydrogen fuel cells could significantly reduce aviation environmental footprint, to the best of the authors' knowledge, the literature seems to lack of studies about hybrid electric configurations using fuel cells instead of batteries for the electrical power generation. Among the few hybrid/full electric aircraft concepts and studies comprising hydrogen fuel cells found in the literature, the most relevant ones are introduced hereafter. ENFICA-FC [11], funded by European Commission, is a project which served to demonstrate through flight tests the feasibility of a full electric 2-seat aircraft based on hydrogen fuel cell power system. HY4 aircraft [12], developed by DLR and manufactured by Pipistrel, is a fuel cell-powered 4-seat passenger aircraft which can be used as electric air taxis. ZeroAvia HyFlier [13] is a zero emission 6-seat airplane which provides a proof-of-concept platform that the company intends to grow into the 15-20 seat platform aimed at the regional airline market (up to 500 NM). These concepts belong to the aircraft category certified according to the CS-23.

The scope of this study is to address the regional aircraft segment certified according to the CS-25 by evaluating the potential of hybrid electric propulsion comprising hydrogen fuel cells for the aforementioned aircraft class. Starting from a baseline conventional turboprop aircraft and replacing its propulsion system with hybrid electric fuel-cell based propulsion, a multidisciplinary design analysis (MDA) process is used to size the propulsion system and evaluate overall aircraft performance in terms of fuel burnt, emissions and energy requirements compared to the conventional kerosene-based aircraft.

The structure of the paper is organized as follows. In Section III, the conceptual aircraft design framework used to design the baseline turboprop aircraft is introduced. The same framework is also used to evaluate the performance of the hybrid electric aircraft. For each discipline, first the methods used for the conventional aircraft are described and then the additional models needed for the fuel cell electric propulsion are presented. Significant weight is given

to the presentation of the models used to perform the hybrid electric aircraft studies. In Section IV, first, the design and the performances of the baseline turboprop aircraft obtained with the aforementioned aircraft design process are shown. Comparison with existing turboprop aircraft of the same category is also provided to validate the design. Then, the parallel hybrid electric architecture selected for this study is presented. The sizing process of the propulsive architecture comprising a conventional gas turbine and a fuel cell system is described together with the hybridization strategy employed during the flight mission. In Section V, the results for the different hybrid configuration are presented. Parametric studies with different hybridization levels and design ranges are carried out to show their impact on the hybrid aircraft performance. Finally a comparison with the baseline aircraft performance is provided. In Section VI, discussion of the results and final conclusions are drawn.

III. Conceptual aircraft design methods

In order to compare the hybrid electric aircraft with a baseline conventional turboprop, a conventional 80 seat twin-propeller aircraft is designed with a conceptual aircraft design platform named *RHEA* design tool. This framework, based on *FAST-OAD*, is a design, analysis and optimization method suitable for both conventional and unconventional regional aircraft configurations. Developed by ONERA and ISAE-SUPAERO, *FAST-OAD* uses a combination of physics-based analyses and empirical correlations for the estimation of aircraft masses, geometry and performance. An exhaustive description of the aircraft sizing process used in *FAST-OAD* is given in [14, 15].

RHEA includes sizing modules for turboprop engines and focuses on the sizing and integration of hybrid electric propulsion configurations. The overall aircraft process used to design the baseline aircraft is illustrated in Fig. 1 with the help of an eXtended Design Structure Matrix (xDSM) scheme [16]. The following paragraphs briefly introduce the methods used in *RHEA* for each discipline. A detailed explanation of all the models is out of the scope of this paper, however references are always provided in order to give the reader a full understanding of the methods used. Nevertheless, exhaustive descriptions are used for the models and the modifications specifically introduced in *RHEA* to size and analyze hybrid electric aircraft using hydrogen fuel cell systems. Most of the equations referenced in this chapter are given in the Appendix (see Section VI).

A. Geometry

1. Initial models in RHEA

The geometry module evaluates aircraft dimensions by decomposing it in five elements: fuselage, wing, horizontal and vertical tail, and nacelle. Each element is initially defined by a set of input parameters which feed an iterative sizing process. Fuselage, wing and tails geometries have been obtained using the equations already available in *FAST-OAD* and shown in [17]. However, for the nacelle geometry, different equations were used because more representative of a turboprop engine. The geometry parameters of the nacelle are assumed to be equal to the gas turbine ones which are determined using Eqs. (1) and (2), derived by Raymer [18] (SI units).

$$D_{gt} = 0.241 \left(\frac{P_{gt}}{745.7} \right)^{0.12} \tag{1}$$

$$L_{gt} = 0.105 \left(\frac{P_{gt}}{745.7} \right)^{0.373} \tag{2}$$

At conceptual design phase, the definition of the geometry of each aircraft system is not required since it is not relevant for overall aircraft performance studies.

2. Additional models for hydrogen-based hybrid propulsion

For hydrogen powered aircraft configurations, the geometrical design of the hydrogen tanks has a non-negligible impact on its masses. Therefore, a set of input parameters for hydrogen tank design is required to define its shape. The dimensionless parameters - λ, ϕ, ψ - needed to characterize the shape of the tank are shown in Fig. 2. This mathematical description of the geometry, which corresponds to an elliptical shell with ellipsoidal heads, ensures a flexible design because it can also characterize simpler ellipsoidal ($\lambda = 0$) or spherical ($\phi = 1$, $\psi = 1$, $\lambda = 0$) shapes. These parameters, together with the tank internal volume V_t, are needed to determine the actual dimensions of the tank using Eqs. (40)

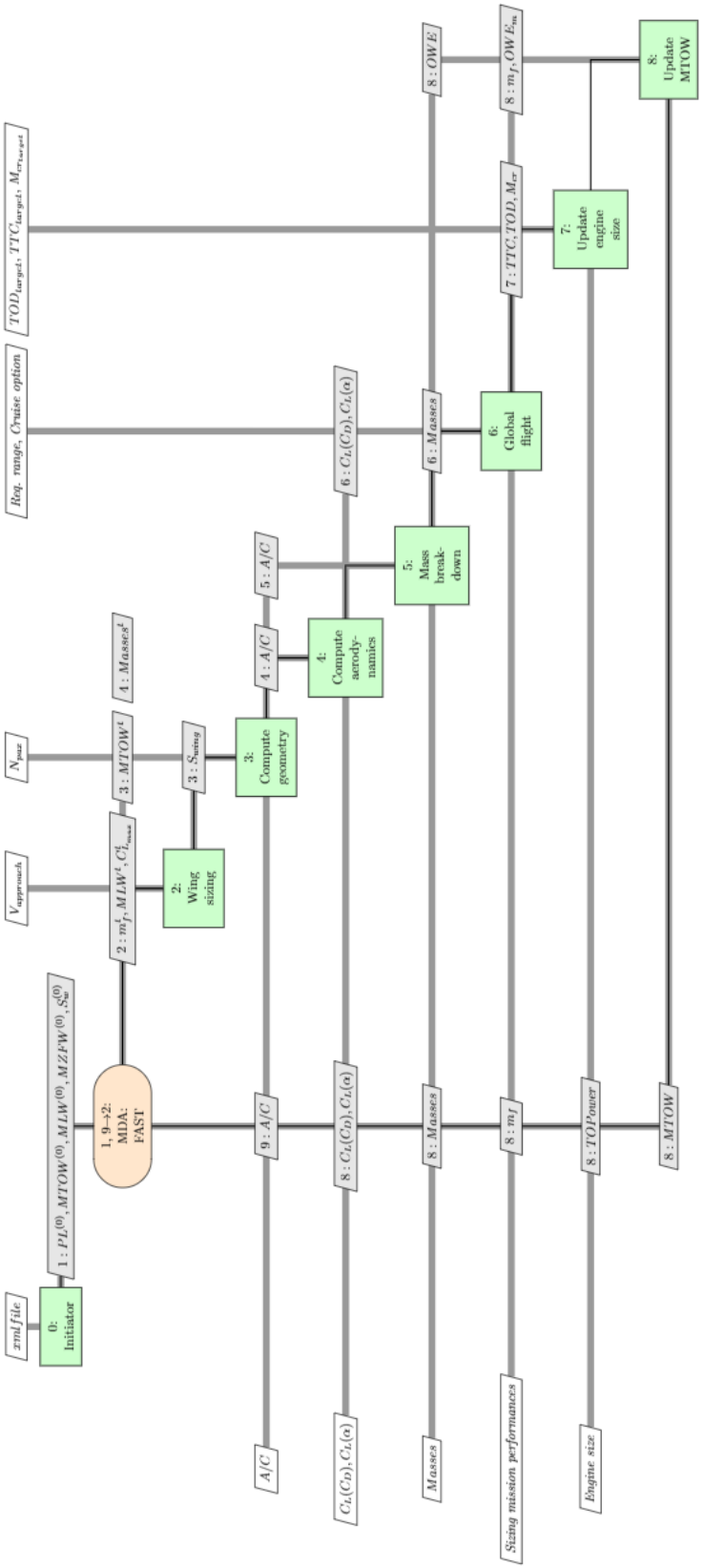

Fig. 1 Baseline Aircraft design process xDSM. Each rectangular box represents an analysis. Input variables related to the analysis are placed vertically while outputs are placed horizontally. The thick gray lines trace data dependencies whereas the thin black lines indicate the data flow. The order of execution is established by the component number.

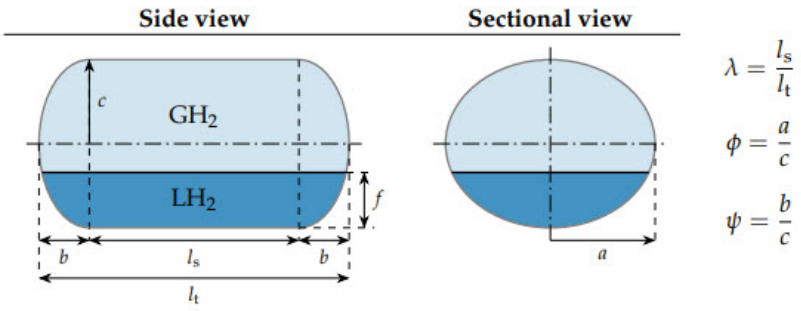

Fig. 2 Parameters defining hydrogen tank geometry [19].

to (43). The tank internal volume V_t is the total volume occupied by the hydrogen and it can be calculated knowing the tank filling pressure p_{fill}, the venting pressure p_v and the mass of hydrogen to be stored given as inputs [19].

B. Masses

For the estimation of the characteristics masses of the aircraft, the mass breakdown used in *RHEA* follows the same standard used in *FAST-OAD* [17], where the operating weight empy (*OWE*) is divided into five parts: airframe, propulsion, systems, operational items and crew. Except for the propulsion, the models used for mass estimation of the components rely on semi-empirical methods collected in the Airbus note [20] or in other aircraft design books such as [18, 21]. For the propulsion part, the method proposed by [22] was used for the prediction of gas turbine and propeller masses.

1. Initial models in RHEA

The conventional propulsion model divides the propulsive unit into four main components: gas turbine including gear box, nacelle, propeller and propulsive control system. The propulsive control system is further decomposed into: engine controls, starting systems and engine provisions (oil system and oil cooler). The total propulsion mass is the sum of each component

$$m_{pp} = m_{eng} + m_{nacelle} + m_{prop} + m_{ps} \tag{3}$$

The mass of each component is evaluated using statistical relations between take-off power and engine mass which are similar to the formula that can be found in Roskam [21] and Raymer [18]. However, some of the methods in these handbooks are somewhat dated, therefore the authors in [22] updated certain models with more recent statistical data for aircraft engines. The trend of engine specific power as function of take-off power, obtained with this method, is illustrated in Fig. 3 for both dry engine and installed engine masses.

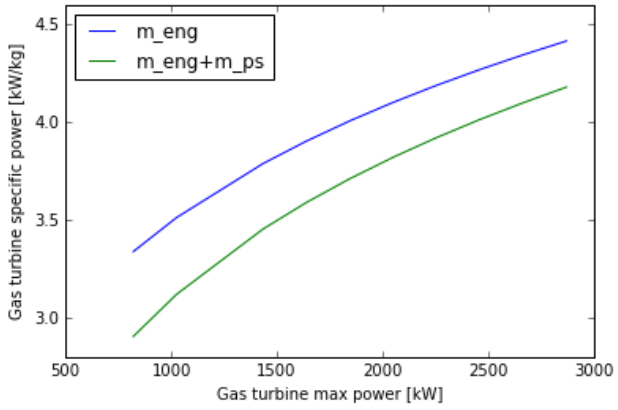

Fig. 3 Gas turbine specific power curves

2. Additional models for hydrogen-based hybrid propulsion

The electric propulsive chain of a fuel cell powered aircraft can be decomposed into five main components: hydrogen storage, fuel cell system, power electronics and electric motor. In order to evaluate the mass of the electric chain, each of these elements has been modelled using physics-based methods as well as published or assumed value of specific power. Additionally, the pipes for H_2 distribution as well as the electric cables and the radiators to dissipate the waste heat produced by the fuel cell have been taken into account for the mass balance of the electric propulsion chain. Assumed values of specific power were used for all the electrical machines (power electronics and electric motor) for which a detailed mechanical modeling is not required since their mass seems to scale linearly with the power. Their masses are therefore given by the following equations:

$$m_{em} = \frac{P_{em}}{P_{sp_{em}}}, \quad P_{sp_{em}} = 7kW/kg \tag{4}$$

$$m_{pe} = \frac{P_{pe}}{P_{sp_{pe}}}, \quad P_{sp_{pe}} = 11kW/kg \tag{5}$$

The assumed values for specific power of these components are representative of state-of-the-art technological levels. Where possible, these values where taken from manufacturer product sheets, otherwise, reasonable values according to some relevant studies from literature were assumed [9, 23, 24].

Concerning the evaluation of the electric cables mass, the results from a study conducted by Vratny [25] were used in order to size the electric transmission cables. Considering the relatively low electric currents required by the electric propulsion system designed for this study, as well as the higher losses caused by the aluminium and the cooling requirements of high temperature superconductors (HTS), the material selected for the evaluation of cables weight is copper. Assuming a total cables length of $30m$, their mass was evaluated using the value of specific mass from Fig. 4.

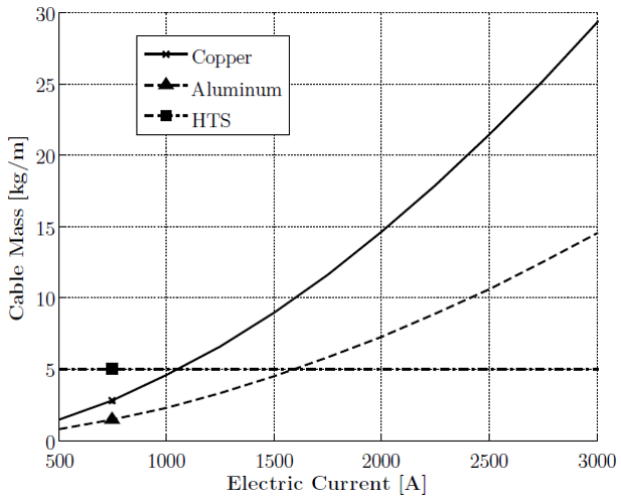

Fig. 4 Specific mass of cables using different conductor material [25]

Different values of specific power for the proton-exchange membrane (PEM) fuel cell system have been found in literature, going from 0.6 kW/kg up to 2 kW/kg [26]. This large discrepancy is due to the diverse kind of applications as well as different fuel cell sizes, for which, the required balance of plant (BoP) components may differ. The balance of plant of a fuel cell is the set of all the required systems and components for the correct functioning of a fuel cell (see Fig. 5). Due to the uncertainty regarding the choice of the right value for fuel cell specific power and considering the huge impact this parameter has on the electric propulsion system mass, it was decided to carry out a component-by-component modeling of the fuel cell system rather than arbitrary choosing a mean value among the ones found in literature.

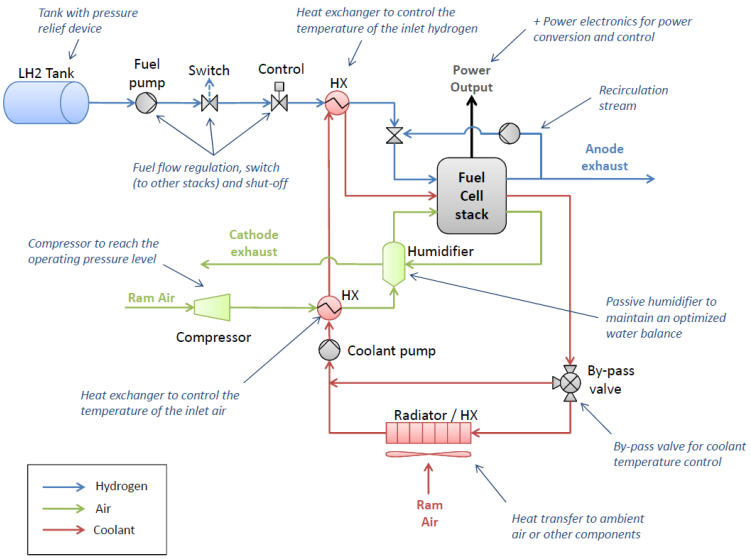

Fig. 5 Schematic layout of the fuel cell BoP including hydrogen tanks.

The method used consists in the development of statistical and analytical relationship for the determination of the mass of each component of the fuel cell balance of plant. Regarding the fuel cell stack, multiple manufacturers (e.g. Ballard, PowerCell) seem to achieve a state-of-the-art specific power of 3.5 kW/kg, for a net power output of 100 kW. According to [27], this value of power is the highest a low temperature PEM fuel cell stack can generate. Therefore, higher levels of electrical power are obtained by connecting in series or in parallel multiple stacks. The specific power of the fuel cell stack is therefore really close to the one of a 2 MW class gas-turbine engine as shown in Fig. 3. However, due to the BoP components, the specific power of the fuel cell system decreases.

In Fig. 5, valves and pressure regulators are required to supply hydrogen to the fuel cell with the right flow rate. In terms of weights, according to [28], each valve weights about $1kg$ and the actuators not more than $3kg$. Therefore, a total of $7kg$ per fuel cell stack (to include inlet and outlet valves) has been considered.

A cooling system is used to dissipate the heat generated by the fuel cell stack and the other components. The mass of the cooling module (coolant, pumps, air/hydrogen heat exchangers) is calculated based on the results from the *Inn-Balance fuel cell project* [29] using the following equation:

$$m_{cool} = \frac{P_{fc}}{P_{sp_{cool}}}, \quad P_{sp_{cool}} = 5.56kW/kg \tag{6}$$

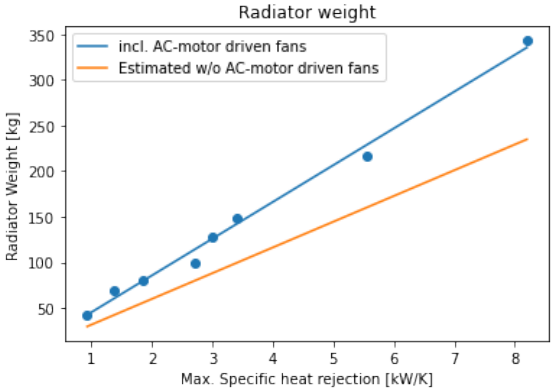

Fig. 6 Empirical laws for the estimation of radiators weight.

Ram air can be used to take heat away from the coolant through air-liquid heat exchangers, known as radiators. The radiator mass $m_{radiator}$ is calculated separately, and will not be included in the fuel cell balance of plant. The cooling ability is directly determined by the specific heat rejection, the temperature of the coolant $T_{coolant}$ and total temperature T_{air}^{tot} of ram air

$$Q_{RAHX} = \text{Specific heat rejection} \times (T_{coolant} - T_{air}^{tot}) \tag{7}$$

The specific heat rejection, whose unit is kW/K, is related to the size and type of radiator. In this study, data sheets from commercial products [30] have been used to derive the sizing laws. The weight variations with specific heat rejection are illustrated in Fig. 6. When the aircraft is operating the fuel cells in static conditions, fans are required to provide sufficient airflow to the radiators. However, restricting the fuel cell system operation to in-flight conditions would allow to considerably reduce the weight of the assembly. The weight savings due to the removal of electric motors and fans from the radiator assembly are estimated to be around 30%.

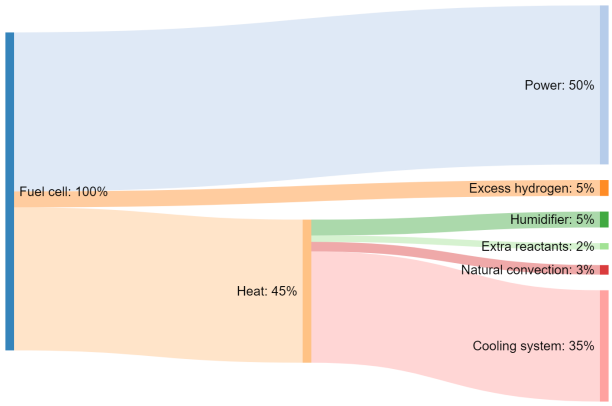

Fig. 7 Energy flows for a typical PEM fuel cell, derived from [31, 32]

Figure 7 presents the heat flows inside a typical fuel cell system. Part of the generated heat is removed from the stack by the extra air and hydrogen that have not reacted, while some may be used to vaporize the product water for the inlet air humidification. Natural convection from the fuel cell body removes a few additional percent of the heat. Finally, about 35% of the incoming hydrogen energy must be rejected as heat by the liquid cooling system [31, 32]. However, part of the waste heat from the fuel cells can be recovered in order to vaporize and heat the cryogenic hydrogen prior to its reaction in the fuel cell stacks. Based on the cooling ability of hydrogen, the required hydrogen flow rate and the required temperature increase fixed by the fuel cell operating temperature, it was estimated that around 13% of the heat to be rejected by the liquid cooling system could be recovered for hydrogen heating and vaporization.

On the cathode side, the reactant air is supplied by a compressor and humidified in a humidity exchanger to prevent the fuel cell membrane from drying, which would reduce the efficiency of the stack. The humidifier mass is scaled from experimental and commercial products (Fig. 8a). The compressor weight is estimated from a linear interpolation over the results from Teichel [33]. The preliminary design carried on by Teichel leads to a relation between the mechanical power of a single-stage axial compressor and its weight, as depicted in Fig. 8b. The mechanical power of the compressor is derived from thermodynamics relations. Given the fuel cell power P_{fc} and the average cell voltage V_{cell}, the air mass flow needed to supply the fuel cell with the oxygen for the reaction with hydrogen is calculated based on the following equation provided by Larminie [35]

$$\dot{m}_{air} = \frac{2P_{fc}3.57 \times 10^{-7}}{V_{cell}} \tag{8}$$

The temperature variation is obtained from the pressure ratio β, the compressor efficiency η and the inlet air temperature T_{in} as shown in the following equation

$$\Delta T = \frac{T_{in}}{\eta}(\beta^{\frac{\gamma-1}{\gamma}} - 1) \tag{9}$$

Finally, the mechanical power is proportional to the flow rate and the temperature variation

$$P_{cmp} = C_p \dot{m}_{air} \Delta T \tag{10}$$

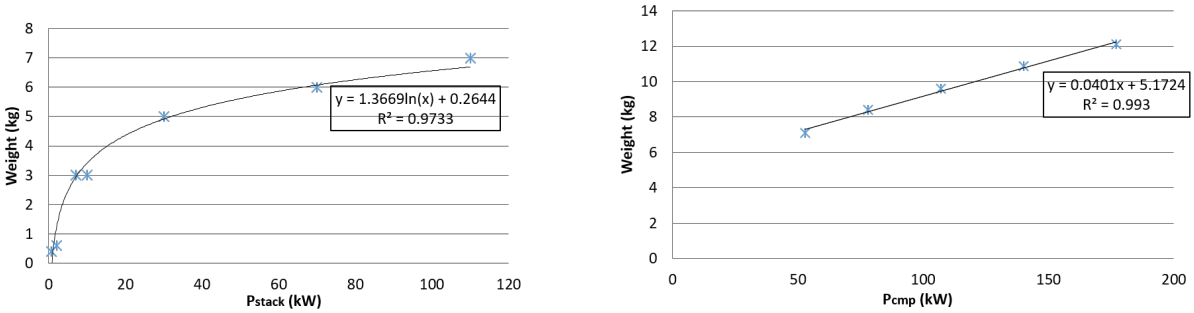

(a) Humidifier weight from Fumatech [34] **(b) Compressor weight from [33]**

Fig. 8 Empirical laws for the estimation of compressor and humidifier masses.

In addition, the mass of the electrical motor driving the compressor has to be taken into account. Teichel [33] provides the following equation for an air-cooled electric motor

$$m_{em}[kg] = 6.08 + 0.077\frac{P_{cmp}}{\eta_{em}}[kW] \tag{11}$$

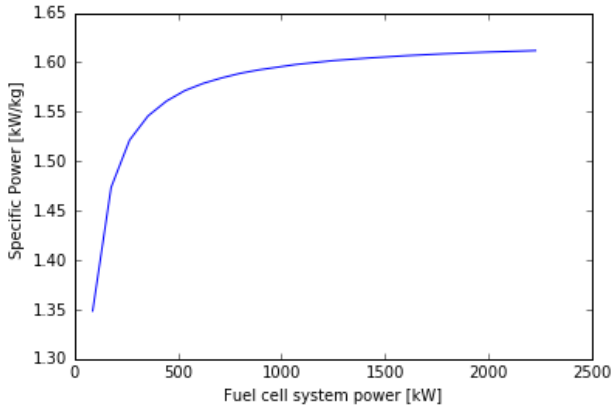

Fig. 9 Fuel cell system specific power trend with fuel cell power (radiator mass not included).

The sum of all these components masses gives the total mass of the fuel cell system

$$m_{fc} = m_{stack} + m_{humidifier} + m_{cmp} + m_{cool} + m_{acc} \tag{12}$$

The resulting fuel cell specific power is shown in Fig. 9 as a function of the net output power. From the results, it can be observed that there is a scaling effect since the higher the power, the better the specific power. Indeed, not all the components masses scale directly with the output fuel cell power, moreover some of these components may be used by multiple stacks. For example, a fuel cell system of 2 MW is actually composed of 20 fuel cell stacks of 100 kW and each stack needs cooling, pumps and all the other components as shown in Fig. 5. Nevertheless, instead of using one compressor for each stack, a single bigger compressor may be used to supply pressurized air to all the stacks, reducing significantly its impact on the total mass of the system.

The model used to evaluate the cryogenic hydrogen tank mass, derived from [19], takes as inputs the total hydrogen mass to be stored and the tank shape as defined in Section III.A. Based on the maximum allowable pressure inside the tank (venting pressure limit), the tank material and the geometry, the model yields to the calculation of the wall thickness, using respectively Eq. (51) or Eq. (49) for an ellipsoidal or a spherical shape. Finally, a thermal analysis provides a relation between the thickness of the insulation and the hydrogen boil-off resulting from the heat leaks.

For this study, a single-layer foam insulation is modeled, which offers low thermal conductivity, reduced weight, and sufficient damage resistance [36]. In order to determine the boil-off losses, thermodynamic equations have been used to calculate the heating flux Q that is exchanged across the tank wall and insulation. The following phenomena have been taken into account:

- internal heat convection between hydrogen and internal surface of tank wall;
- heat conduction through the tank wall;
- heat conduction through the insulation material;
- external heat convection between air outside the tank and the external surface of tank insulation.

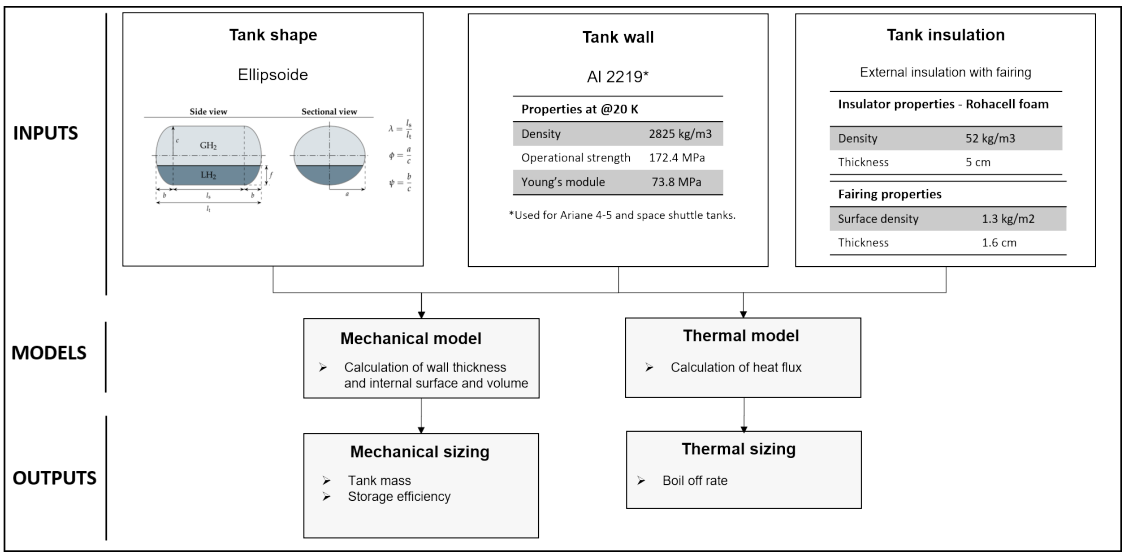

Fig. 10 Flowchart of tank design

The model calculates the temperature value at each interface and, consequently, the heat exchanged through the tank. Then, knowing the hydrogen latent heat of vaporization λ_{H_2}, the boil-off rate is calculated as follows

$$BOR = \frac{Q}{\lambda_{H_2}} \tag{13}$$

The full set of equations used to determine the hydrogen tank mass can be found in Section VI. A simplified flowchart with the main inputs used for this study is shown in Fig. 10. In order to choose the input tank shape parameters, a sensitivity analysis was performed to evaluate the dependency of the storage efficiency on the shape parameters. The storage efficiency is defined as in Eq. (14). Due to its low area-to-volume ratio, the spherical shape clearly offers the best solution in terms of weight, volume and heat loss. However, the integration of such tanks in the aircraft is not practical, therefore cylinders with rounded edges ($\psi = 1$) are preferred. Results of the sensitivity study in Fig. 11 show that a cylindrical shell ($\phi = 1$) provides a much better storage density than elliptical ones ($\phi \neq 1$). The parameter λ has a lower impact on the storage efficiency. Moreover, while a greater value of λ provides a slightly better efficiency, it also increases the boil-off rate as shown in Fig. 12. Therefore, the choice of λ must result from a trade-off between tank mass and boil-off requirement, but could also be derived from operational as well as installation constraints. For this study, a value of $\lambda = 0.5$ is chosen. The full set of shape parameters is therefore selected: $\lambda = 0.5$, $\phi = 1$ and $\psi = 1$. The choice of these parameters, together with the previously shown assumptions regarding tank wall material and tank insulation, gives the tank storage efficiency as a function of tank capacity as illustrated in Fig. 11

$$\eta_g = \frac{m_{H_2}}{m_{H_2} + m_{tank}} \tag{14}$$

Hydrogen distribution from the cryogenics tanks to the fuel cell stacks is ensured by cryogenic pipes with Rohacell ® foam insulation. This type of insulation has been selected being lightweight, cheap and with good mechanical properties. Other insulation architectures exist in the literature but provide limited properties (e.g. Aerogel ®) or operate in peculiar conditions which would require an efficient monitoring to prevent failures (e.g. multi-layer insulation). The preliminary

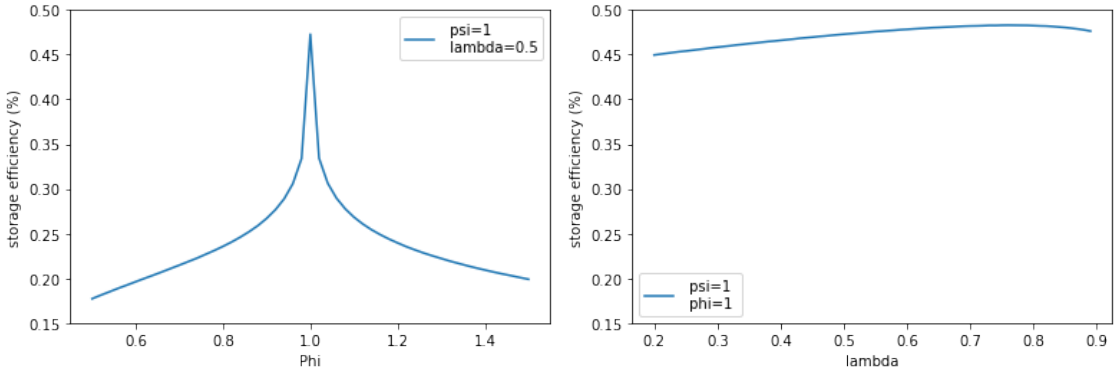

(a) Evolution of η_g with ϕ **(b) Evolution of η_g with λ**

Fig. 11 Dependency of storage efficiency on the shape parameters for a tank capacity of 60 kg of H_2.

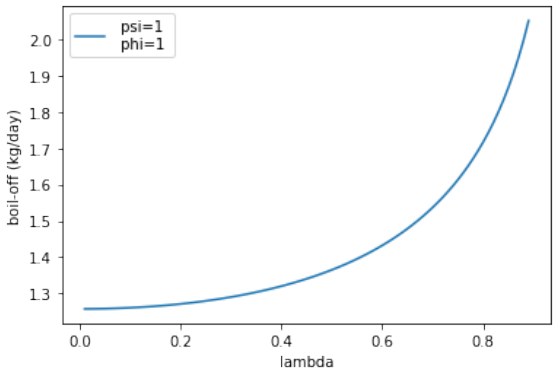

Fig. 12 Dependency of boil-off rate on λ

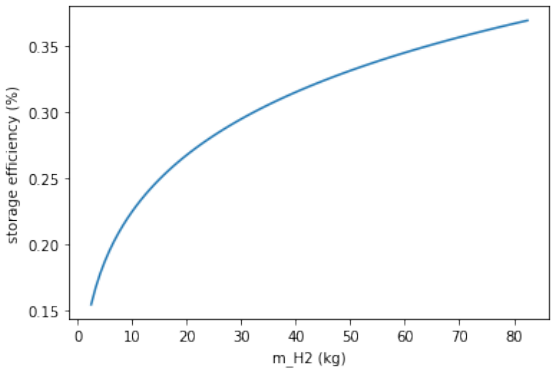

Fig. 13 Scale effect of η_g with tank capacity

design of Rohacell ® foam insulated pipes is done in two steps. First, the inner diameter of the pipes is derived from the flow rate, according to the method proposed by [37]. Then, a heat transfer analysis is performed to evaluate the performance of the insulated pipes. The model evaluates the mass of the pipes (m_{distr}), by evaluating the mass of the pipe wall and of the required insulation layer and assuming a total required length of $50m$.

The results in terms of specific mass variation with hydrogen flow rate are shown in Fig. 14. This includes a pipe wall made of 304L steel and insulation with Rohacell ® foam.

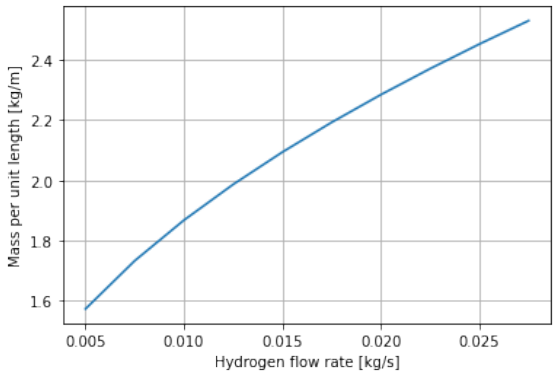

Fig. 14 Pipe specific mass variation with hydrogen flow rate

C. Aerodynamics

1. Initial models in RHEA

The aerodynamics module consists of low fidelity models based on semi-empirical equations allowing for extremely fast computation of the aerodynamic performance of the aircraft. It is devoted to the computation of the drag polar $C_D = f(C_L)$ for both high speed and low speed conditions. The total drag is decomposed into four components: friction drag D_0, induced drag D_i, wave drag D_w and trim drag D_{eq}

$$C_D = C_{D_0} + C_{D_i} + C_{D_w} + C_{D_{eq}} \tag{15}$$

Each drag component is estimated according to the methods proposed by Roskam [21]. More details about the model and the formulas used can be found in [17].

2. Additional models for hydrogen-based hybrid propulsion

The cooling system of the electric power-train installed inside the aircraft requires a certain amount of external air-flow to evacuate the heat produced in order to keep all the systems at their operational temperature. Therefore air scoops are needed in order to provide the required air-flow to the systems. Moreover, air scoops are also required in order to supply the fuel cells with the required amount of oxygen to react with hydrogen in order to generate electrical power. These air scoops are responsible for a degradation of the aerodynamic performance of the aircraft. However, the aerodynamics penalties due to the presence of ram air inlets were not taken into account at this stage and only the mass of the required cooling systems were evaluated. Therefore, additional methods for the evaluation of the drag penalties to be taken into account to provide the required air-flow have not been developed.

D. Propulsion

1. Initial models in RHEA

The propulsion module includes all the methods for the estimation of propulsion performance in terms of fuel consumption and emissions. The gas turbine model consists in the characterization of a twin-shaft free turbine engine architecture (see Fig. 15). This configuration was chosen because representative of the PW100 aircraft engine family, used by a large number of turboprop aircraft and which covers a wide power range between 1100 to 3700 kW. Assuming that these engines have similar designs, the model can scale the engine to lower or higher powers within the PW100 engines power range, while providing the same specific fuel consumption.

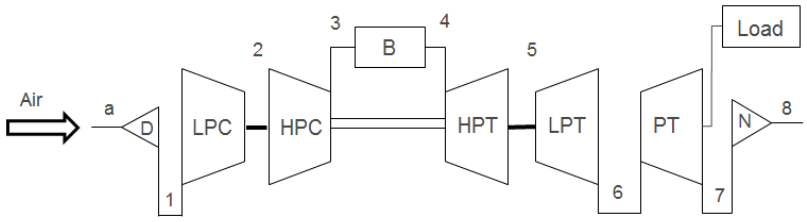

Fig. 15 Gas turbine architecture

The model evaluates the available power and the specific fuel consumption by computing the thermodynamic properties of the air flow at the inlet and the outlet of each engine component and by solving the power balance equations of the low pressure and high pressure spools. At the design point, available data from the engine's manufacturer were used to characterize engine's components, such as compressor pressure ratios, max turbine inlet temperature and compressors' bleed airflow. The component efficiencies were estimated using representative values relative to the state-of-art engine technology according to [38]. The off-design analysis is performed following the method described by Mattingly [38] and Oates [39]. The components efficiencies are assumed to be constant, therefore no scaled performance characteristics are calculated from the original performance maps. The off-design performance is calculated only by considering relations related to the gas-generator's turbine and compressor matching and the power turbine and exhaust

nozzle matching. Simulation results of this rubber engine model are shown in Fig. 16, where power specific fuel consumption is plotted against altitude for different values of Mach number and throttle.

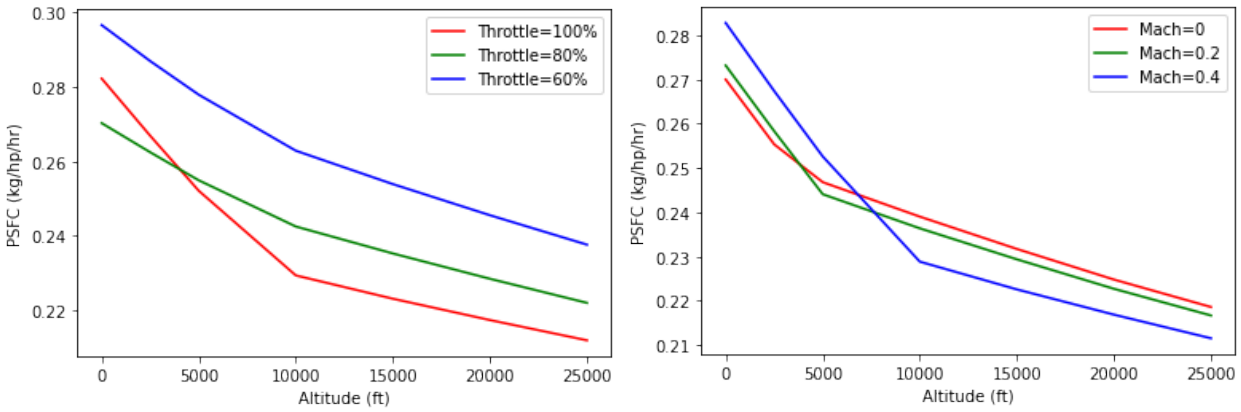

(a) SFC at cruise rating at Mach=0.45

(b) SFC at max climb rating

Fig. 16 Gas turbine specific fuel consumption for different ratings

The thrust produced by the propeller is evaluated using Eq. (16), where the propeller efficiency is determined at each condition during the flight mission using a simple model based on the actuator disk theory (ADT) for a propeller sized for a max shaft power of $1.1P_{gt_{RTO}}$

$$T = (\eta_{prop} P_{shaft})/speed \tag{16}$$

For takeoff performance, when the aircraft speed is close to 0, Eq. (16) is not applicable. The actuator disk theory can be considered valid starting from Mach values of 0.2. A linear interpolation model between the static thrust value evaluated using the following equation proposed by [40] and the thrust at Mach 0.2 evaluated with the ADT model has been used in order to estimate the thrust for all the Mach numbers between 0 and 0.2

$$T_0 = \frac{K_{T_0} P_{shaft}[hp]}{rpm \times d_{prop}[ft]} \tag{17}$$

where T_0 is the static thrust in pounds and K_{T_0} is the static thrust coefficient which according to [40] was estimated to be 55000.

2. Additional models for hydrogen-based hybrid propulsion

The determination of hydrogen consumption is given by the overall efficiency of the electric propulsive chain

$$\dot{m}_{H2} = \frac{P_{shaft}}{\eta_{fc}\eta_{pe}\eta_{em}FHV_{H2}} \tag{18}$$

Both the electric motor and power electronics efficiencies were assumed to be constant and equal respectively to 97% and 98%, which are representative values of state-of-the-art technology levels [9]. A different approach, involving an in-depth modeling of a fuel cell based on thermochemical equations, was used to evaluate fuel cell system efficiency. As shown in Fig. 5, a fuel cell system is composed of a fuel cell stack and of a certain number of components which significantly increase the mass of the fuel cell, but also use some of the output electrical power of the fuel cell stack to work. Therefore, the net output power of the fuel cell system P_{fc} is lower than the gross output power of the fuel cell stack P_{stack}. In terms of efficiency, it translates into the following mathematical formulation

$$\eta_{fc} = \eta_{stack} \frac{P_{fc}}{P_{stack}} \tag{19}$$

As shown by [25], the main power consumer of the BoP is the compressor. For this study, all the secondary power consumers have been neglected. The compressor power requirement is calculated using Eq. (10). With this method, the

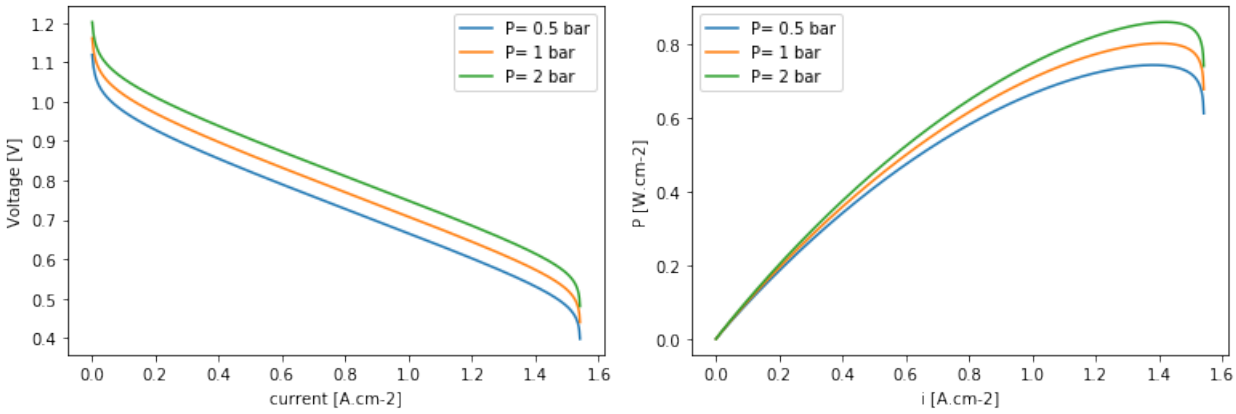

(a) Fuel cell polarization curves **(b) Fuel cell power curves**

Fig. 17 Dependency of fuel cell polarization curve and power on operating pressure

resulting ratio between net and gross output power is $\frac{P_{fc}}{P_{stack}} = 0.89$. Finally, Eq. (20) is used to evaluate the fuel cell stack efficiency

$$\eta_{stack} = \eta_{cell} = \eta_{ideal} \frac{V_{net}}{E_{OCV}} \tag{20}$$

where V_{net} is the fuel cell net output voltage and E_{OCV} is the fuel cell open circuit potential. The ideal fuel cell efficiency at standard condition is obtained by dividing maximum work output by the enthalpy input (Eq. (21)). In this ideal conditions, the fuel cell reversible potential E_r is given by:

$$\eta_{ideal} = \Delta G / \Delta H = 83\% \tag{21}$$

$$E_r = -\Delta G / nF = 1.229V \tag{22}$$

At non-standard conditions, E_{OCV} is given by:

$$E_{OCV} = E_r + \frac{\Delta S}{2F}(T - T_{ref}) + c \log(P/P_{ref}) \tag{23}$$

V_{net} is evaluated considering the voltage losses due to $v_{activation}$, v_{ohmic} and $v_{concentration}$, obtained using the following equations:

$$v_{activation} = \frac{2RT}{nF} sinh^{-1} \frac{i}{2i_0} \tag{24}$$

$$v_{ohmic} = iR_{ohmic} = i(R_{elec} + R_{ionic}) \tag{25}$$

$$v_{concentration} = \frac{2RT}{nF}(1 + \frac{1}{\alpha}) log \frac{i_l}{i_l - i} \tag{26}$$

$$V_{net} = E_{OCV} - (v_{concentration} + v_{activation} + v_{ohmic}) \tag{27}$$

These voltage losses are function of the current density. The evolution of the net voltage against the current density is known as polarization curve and is an important indicator of the fuel cell performance. Figure 17a shows the resulting polarization curve obtained for different operating pressures.

The polarization curve gives also the trend of the electrochemical efficiency of the fuel cell with the operating current. Since η_{cell} is proportional to V_{net}, the lower the current, the higher the efficiency. As shown in Fig. 17 the maximum power point does not correspond to the maximum efficiency point. The choice of the operating point is not straightforward. Therefore, the optimum operational current is obtained using a weight parameter, w_p, which defines the relative importance of fuel cell power density over the efficiency. With this weight parameter, an overall objective function is calculated

$$f(\eta_{cell}, P_{cell}) = w_p P_{cell} + (1 - w_p)\eta_{cell} \tag{28}$$

If the objective is to optimize only the weight of the fuel cell, then a w_p of 1 should be chosen. Values of w_p between 0 and 1 are chosen if a compromise between maximum power and efficiency is required. For this study, a value of $w_p = 1$ is chosen, resulting in a cell operating voltage of 0.60 Volts and a cell efficiency $\eta_{cell} = 48\%$ at $T = 353\ K$ and $P = 2\ bar$. The overall fuel cell system efficiency including BoP is therefore $\eta_{fc} = \eta_{stack} P_{fc}/P_{stack} = 43\%$. The actual output power of each cell depends on the assumed surface area of the cell. For this study a cell surface area value of $650 cm^2$ was used from estimation of fuel cell manufacturers data sheet [41]. The output power of a single cell at the chosen operating point is approximately 530 W. Therefore, each fuel cell system with a net output power of 100 kW is composed of a fuel cell stack with 211 cells stacked in series, producing a voltage of 127 V and a current of 882 A.

3. Emission model

Emissions are evaluated in terms of CO_2 equivalence (CO_{2eq}), which is a measure of the global warming impact of $GHGs$ gases using the global warming potential (GWP) of CO_2 as reference. The carbon dioxide equivalency for a gas is obtained by multiplying the mass and the GWP of the gas. Table 1 gives the equivalence for the main $GHGs$ gases.

Greenhouse gas	**kg CO_{2eq}/kg**
CO_2	1
Methane (CH_4)	25
Nitrous oxide (N_2O)	298

Table 1 Global warming potential for 100 years time horizon relative to CO_2 [42].

The method takes into account the combination of all the steps from extracting, capturing or growing the primary energy carrier to refuelling the vehicles with the finished fuel. The combination of all the steps necessary to turn a resource into a fuel and bring this fuel to a vehicle is defined as ”Well-to-Tank” pathway (WTT). Instead, the utilization of this fuel within the air-vehicle is referred to as ”Tank-to-Wake” pathway (TTW). The sum of WTT and TTW emissions is defined as "Well-to-Wake" pathway (WTW). In [43], WTT emissions have been accurately calculated for different hydrogen pathways, each of them being identified by a code. The most representative pathways have been chosen for the main primary energy sources, such as: natural gas, coal, biomass (waste wood), wind. Figure 18 shows the energy expended and the WTT greenhouse gases emitted for the chosen pathways. Each pathway is described in detail in [43].

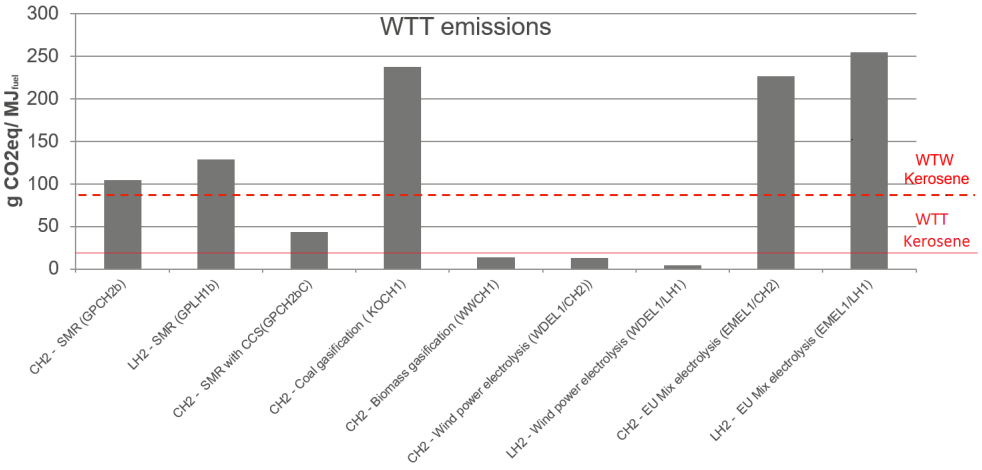

Fig. 18 WTT $GHGs$ emissions of hydrogen pathways.

As it can be seen in Fig. 18, due to the high energy demanding process for producing hydrogen, related emissions can be as high as twice the ones coming from the entire kerosene cycle (from production to combustion). Only if green energy sources are used, these emissions can actually be reduced, which is the case for biomass and wind. For this study, the emission index used for the calculation of WTW emissions of Jet-A fuel and liquid hydrogen are respectively 88.6 and 4.2 $gCO_{2eq}/MJfuel$. For the hydrogen related emissions, the selected index corresponds to the WTT emissions of

the LH_2 wind power electrolysis pathway. The only product of the reaction between hydrogen and oxygen within the fuel cell is water vapour, therefore the WTW CO_{2eq} emissions correspond to the WTT emissions shown in Fig. 18 for the selected pathway. In addition to the production of CO_{2eq}, the model also evaluates H_2O and NO_x emissions. The indexes used to calculate these emissions are summarized in Table 2. NO_x formation from Jet-A combustion does not exclusively depend on the amount of nitrogen in the fuel but also on the air-fuel mix ratio. High temperatures and oxidation-rich conditions generally favour NO_x emission in combustion. Therefore, the correlation for the NOx emission index (kg NO_x/kg fuel) is calculated as a function of burner entrance pressure (kPa) as well as combustion chamber entrance and exit temperatures (K), as shown in the following equation:

$$EI_{NOx} = 5.4728 \times 10^{-9} T_4 P_3^{0.37} e^{\frac{T_3}{191.67}} \tag{29}$$

Jet-A emission indexes	
$EI_{CO_{2eq}}$	3.76 kg CO_{2eq}/kg Jet-A
EI_{H_2O}	1.26 kg H_2O/kg Jet-A
Hydrogen fuel-cell emission indexes	
$EI_{CO_{2eq}}$	0.5 kg CO_{2eq}/kg H_2
EI_{H_2O}	9 kg H_2O/kg H_2

Table 2 Fuel-specific emission indexes

Concerning H_2O emissions, assuming rough values of gas turbine efficiency η_{gt} of 30% and fuel cell efficiency η_{fc} of 50%, in order to produce the same amount of propulsive energy, hydrogen fuel cells emit roughly 50% more water vapor than a conventional kerosene gas turbine.

– Kerosene gas turbine H_2O emissions

$$\frac{EI_{H_2O}}{FHV_{Jet-A} \times \eta_{gt}} = 0.35 g H_2O/Wh \tag{30}$$

– Hydrogen fuel cell H_2O emissions

$$\frac{EI_{H_2O}}{FHV_{H_2} \times \eta_{fc}} = 0.54 g H_2O/Wh \tag{31}$$

However, water vapor emissions are not considered as an environmental concern for different reasons. The residence time of water vapor emitted at the typical cruise altitude of turboprop aircraft is of a couple of weeks. For comparison, the residence time for CO2 is of 100 years, so the environmental impact of CO_2 emissions is a function of the total emission over the past 100 years. Moreover, the direct radiative effect of water vapor emissions is believed to be negligible [44, 45]. The primary concern about water vapor emissions is the indirect effects which are complex and uncertain, one of these being contrails formation. However:

– "*Contrails formation do not scale directly with the amount of H_2O emitted because aircraft H_2O emissions just act as a trigger for contrail formation*" [44]: more H_2O emissions do not imply more or bigger contrails.

– "*Contrails formation depend on what is emitted from the engines in addition to water vapor*" [44]: the only emission of hydrogen fuel cells is water so the absence of sulfurs compounds should reduce the probability of contrails formation.

To conclude, it seems reasonable to assume that, at the typical flight altitudes of the considered aircraft class, an increase of water vapor emissions of 50% would not have a significant environmental impact and therefore will not be used as performance metric for the following preliminary studies.

E. Performance

Based on a segment-by-segment simulation using time step integration, the performance module solves the equations of motion to evaluate the performance of the vehicle throughout the mission in terms of fuel consumption and emissions. For the conventional aircraft flight mission, no particular modifications were applied to the existing performance module of *FAST-OAD* as described in [17]. For each time step the performance module performs the analyses illustrated in Fig. 19 using an eXtended Design Structure Matrix (xDSM) scheme [16]. Under this format, each rectangular box represents an analysis (e.g. a function or computational model). Input variables related to the analysis are placed vertically while outputs are placed horizontally. The thick gray lines trace data dependencies whereas the thin black lines indicate the data flow. The order of execution is established by the component number. However, for the hybrid

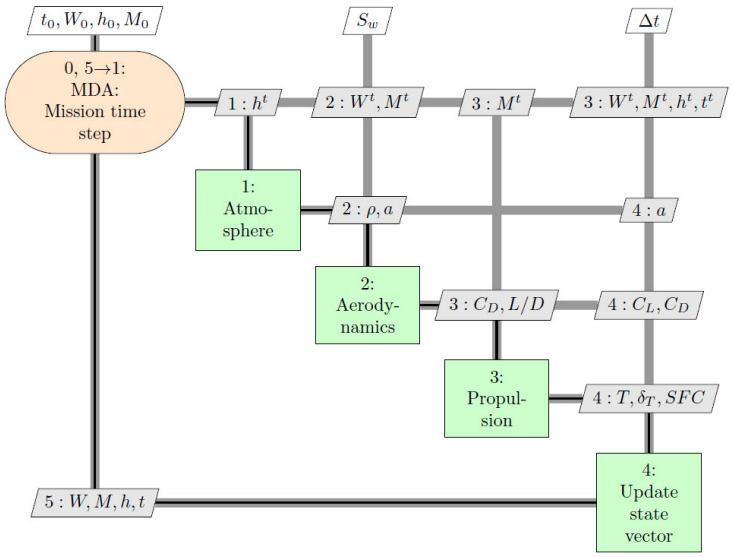

Fig. 19 xDSM diagram for the time step performance analysis [17].

electric aircraft mission in *RHEA*, some modifications were required. At each time step, the hybrid aircraft is not only consuming kerosene, but also hydrogen, therefore the mass variation of the aircraft at each time step takes into account both jet fuel consumption and hydrogen consumption.

IV. Aircraft models

In this section, the aircraft design process introduced in Section III is used to design the baseline turboprop aircraft which will serve as baseline for all the hybrid-electric configurations studies. Input data and TLARs used to initialize the design process have been derived, where possible, from publicly available data of the ATR72 aircraft, since this aircraft is considered the most representative of the regional turboprop market with more then 75% of market share. The resulting aircraft model is then compared to the ATR72 aircraft in order to provide a general validation of the design process and to check the validity of the design. Then, the hybrid electric aircraft model is built by replacing the conventional turboprop engine with a parallel hybrid architecture described hereafter. Therefore, between the baseline aircraft and the hybrid aircraft there are no differences in terms of geometry, airframe and systems masses which are not related to the propulsion system. Employing this design approach, several hybrid aircraft configurations are sized with respect to various design parameters such as design range, power hybridization factor and hybridization strategy. Nevertheless, they all share the same propulsive architecture described in Section IV.B.

A. Baseline Aircraft

The main top level aircraft requirements given as inputs to the aircraft design process shown in Section III are given in Table 3. Additional inputs required by the design process are the set of geometrical parameters for the preliminary sizing of the wing, the tails and the cabin as well as the set of design parameters for the sizing of the turboprop engine. These inputs have not been included in the table for the sake of simplicity since their definition is not particularly

relevant to the scope of the studies of this paper.

TLARs	
Number of passengers	72
OEI net ceiling	>2900 m
Take off distance	<1200 m
Time to climb to FL200	<24 min
Approach speed	116 $knots$
Max cruise Mach @MTOW	0.45
Design range @72PAX	750 NM

Flight mission inputs	
Min. control speed (V_{MCA})	99 $knots$
Climb speed	170 $knots$
Cruise flight level	20000 $feet$
Diversion distance	100 NM
Diversion flight level	14000 $feet$
Diversion cruise Mach	0.33
Holding duration	30 min

Table 3 Top level aircraft requirements and inputs paramaters

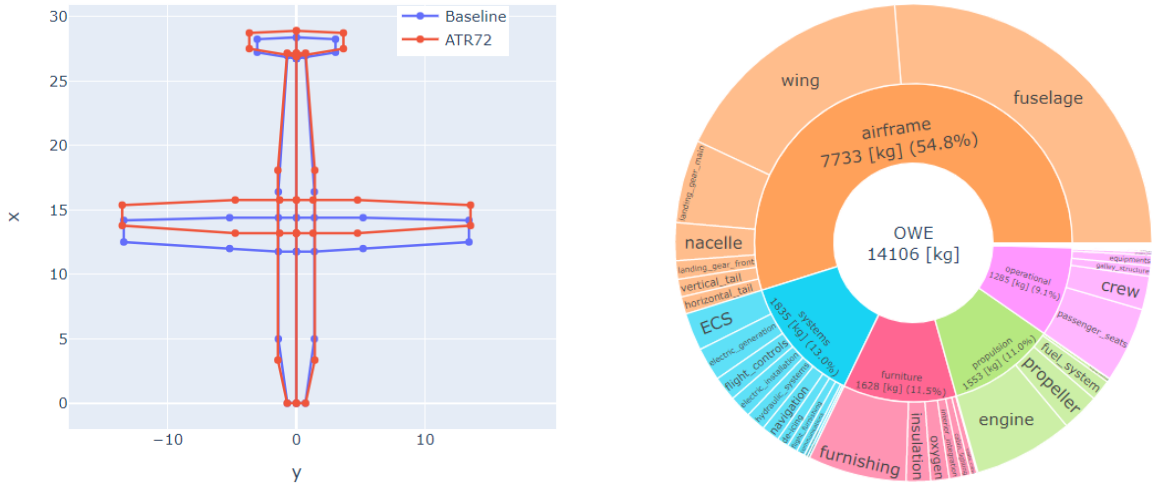

(a) Baseline aircraft geometry compared to the ATR72

(b) Weight breakdown of the baseline aircraft

Fig. 20 Main dimensions and weight breakdown of the baseline aircraft

Parameter	ATR72 [46]	Baseline aircraft	Delta
MTOW	23000 kg	23572 kg	+2.5%
OWE	13500 kg	14106 kg	+4.5%
Wing area	61 m^2	59.9 m^2	-1.8 %
Take-off Power	2475 hp	2415 hp	-2.4%
Fuel flow at cruise speed	762 kg/h	699 kg/h	-8.3 %
Cruise glide ratio	Not disclosed	15.7	N/A
Block fuel for 200NM	618 kg	587	-5%
Block fuel for 300NM	859 kg	849	-1.2%

Table 4 General aircraft characteristics

The main dimensions of the baseline aircraft and the obtained weight breakdown are shown in Fig. 20. The flight profile of the design mission is shown in Fig. 21. Moreover, in Table 4 general characteristics of the obtained aircraft design are also compared with published data of the ATR72 in order to ensure the validity of the resulting design. As it

can be seen in the table, the discrepancies are relatively low, with the highest deltas being less than 10%. More accurate results may be obtained by using calibration factors to apply, for example, to engine performance parameters. However, such faithful reproduction of the original ATR72 aircraft is out of scope, therefore the obtained turboprop aircraft design can be considered as a valid representation of a 70-seat turboprop aircraft. Flight mission simulations of the baseline aircraft have been performed for three different flight distances (200NM, 400NM and 600NM) at the maximum cruise speed and with the flight mission parameters defined in Table 3. The results of these simulations will serve as reference for the parametric studies with hybrid-electric propulsion presented in the next section.

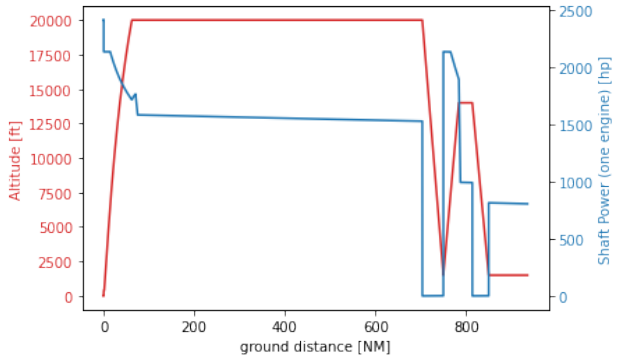

Fig. 21 Baseline aircraft flight profile of design mission

B. Hybrid aircraft

The hybrid electric aircraft model is designed starting from the characteristics of the baseline turboprop aircraft presented in the paragraph above. Thus, the design process takes as inputs all the geometrical characteristics as well as the mass breakdown and the aerodynamic performance of the baseline aircraft. Only the hybrid propulsive architecture is designed and sized according to different parameters. Different propulsive layouts may be used to design a power-train comprising fuel cells to generate electrical power: full-electric, parallel hybrid, series hybrid or series/parallel hybrid [47]. The identification of the most advantageous architecture is a complex task which is influenced not only by its performance in terms of fuel consumption or emissions, but also by operational and integration constraints which must be identified and quantified for each architecture. However, a comprehensive investigation of the most promising architecture is out of the scope of this study. The objective of this paper is rather to give an idea of the potential of fuel cell technology to reduce the environmental impact of a large turboprop aircraft by performing parametric studies for a defined set of parameters. Therefore, a single architecture was selected to perform the study. The choice was made based on previous studies and preliminary considerations. The full-electric configuration was discarded because it was estimated that the volume occupied by the hydrogen tanks and the fuel cell system would represent a significant installation constraint. Moreover, safety issues arising from the risks of electric arcs and electromagnetic interference related to the high voltage systems would represent a big challenge for all-electric aircraft. An hybrid electric architecture comprising both a conventional gas turbine and a fuel cell system represents a more feasible solution in the short-to-medium term, since the power level of the electrical system can be considerably lower with respect to the full-electric configuration, in which, the required propulsive power must be entirely provided by the electrical system. Among the different possible architectures, the parallel hybrid layout was selected. According to previous studies [5, 7], this architecture seems to be the most energy efficient and lightweight, specially if distributed propulsion is not envisaged, which is the case for this study.

Figure 22 shows the parallel hybrid electric configuration chosen for this study. Each propeller is supplied with mechanical power provided by both the electric motor and the gas turbine. The two power contributions to the required total system power are imposed by the power hybridization factor H_P, which is defined as the ratio between the power supplied by the electric motor and the total power transferred to the propeller. The electric motors converting the electrical power into mechanical power, are alternating current (AC) motors which, compared with direct current (DC) motor drives, show several advantages such as lightweight, small volume, low cost, and high efficiency [48]. However, fuel cells are electrochemical devices providing DC current at their terminals, therefore DC-AC power converters are also needed. The electric core is a DC supply grid which includes power switches and circuit breakers for the

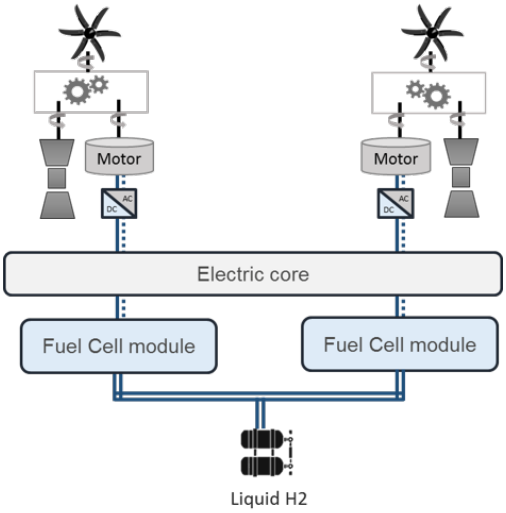

Fig. 22 Schematic layout of the selected parallel hybrid architecture.

protection system as well as all the electronic components needed for power management and control. In this paper, the combination of electric core and DC-AC power converters is also referred to with the more generic term of power electronics. The fuel cell modules which generate the electrical power have the layout shown in Fig. 23a. Each module is composed of a certain number of fuel cell systems connected in series which depends on the max electrical power for which the system has to be designed. The single fuel cell system unit designed for this study has a net power output of 100 kW with the corresponding voltage and current levels respectively of 127 V and 882 A. The evolution of voltage and current values for different power levels of the fuel cell module is given in Fig. 23b in order to give an idea of the order of magnitude of the main properties of the electrical power grid.

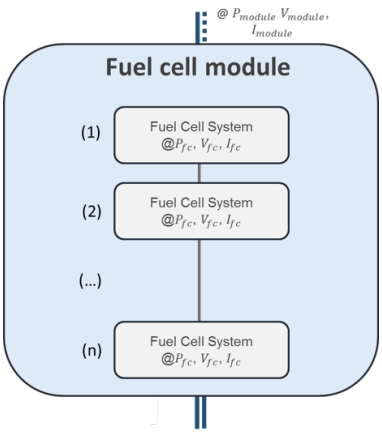

(a) Schematic of the module layout

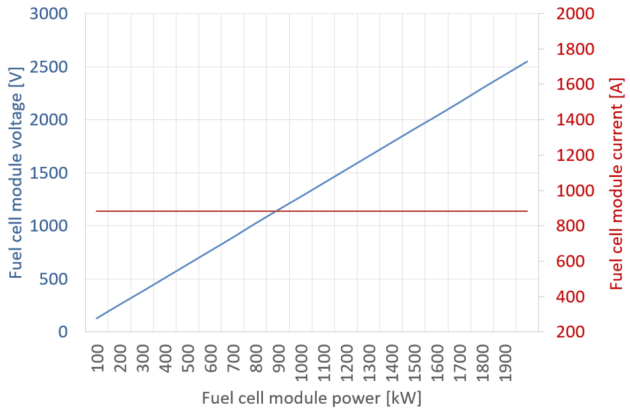

(b) Evolution of voltage and current with fuel cell module power.

Fig. 23 Layout and electrical properties of a fuel cell module.

V. Results

The hybrid propulsive system of the hybrid aircraft is sized relatively to the nominal electric power and the design range given as inputs. According to those inputs, the mass of the entire hybrid propulsive system is determined using the methods described in Section III. Due to the inevitable increase of OWE caused by the higher mass of the hybrid propulsive architecture, in order to comply with the characteristic $MTOW$ of the baseline aircraft, the maximum payload is reduced accordingly. Therefore, for the hybrid electric aircraft design process, the number of passengers is not a

given requirement, but rather an output of the process. The total take off power of the hybrid aircraft is kept equal to the take off shaft power of the baseline aircraft, therefore the definition of the nominal electric power implies also, by means of a simple arithmetic operation of subtraction, the definition of the gas-turbine take off power. Thus, the hybridization factor, H_P, at take-off is only function of the electric power, given that the total installed power does not change.

Concerning the hybridization strategy, i.e. the power management strategy of the two power sources throughout the mission, the chosen approach consists in the full exploitation of the total power available during the flight phases of climb and cruise, whereas during the descent phase only the gas-turbine is employed at idle rating. As a result, the hybridization factor will be slightly higher at higher altitudes since the available gas-turbine power decreases due to the effect of lower air density while the electrical power output is not affected by the atmospheric conditions. Nevertheless, two different approaches are still viable: the first consists in the exploitation of electric power during all flight phases of climb and cruise, including diversion and holding, whereas with the second solution, the electric power will be used only during the climb and cruise phases of the design mission, leaving the gas-turbine to provide with the required power throughout the reserve flight. For the sake of simplicity, these two approaches will be referred to as "full hybrid mission" and "main hybrid mission", respectively.

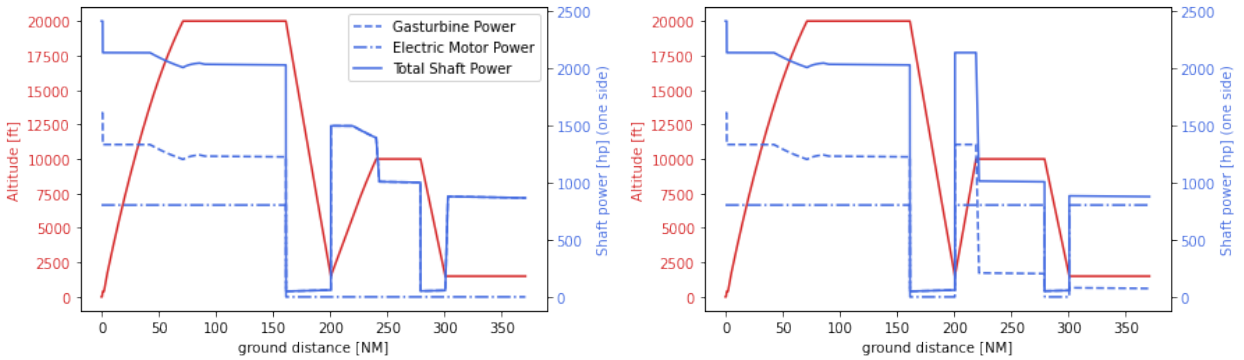

(a) Flight power profile for main hybrid mission **(b) Flight power profile for full hybrid mission**

Fig. 24 Representation of power management for two hybridization strategies

In Fig. 24, the flight power profiles for both strategies - for a design mission of $200NM$ with a nominal electrical power of $600kW$ per side - are illustrated in order to give a better understanding of the concepts explained. Hybrid aircraft flight simulations are always performed with the same speeds and altitudes as the ones used for the baseline aircraft (illustrated in Table 3). However, the diversion cruise altitude was reduced to $10000ft$ and its speed to a Mach number of 0.25, in order to allow sufficiently high hybridization factors, which would otherwise lead to insufficient gas-turbine power levels to perform the reserve flight.

A parametric study with the hybridization factor varying approximately between 0.1 and 0.5 (corresponding to nominal electric power varying between $200kW$ and $1200kW$) was conducted for both strategies for a design range of $200NM$ and the most relevant results are illustrated in Fig. 25. The graph on the left hand side shows that the mass penalty due to the installation of the hybrid electric architecture does not vary significantly with the choice of the hybridization strategies investigated herein. Indeed, for each specific hybridization factor, the only difference in the propulsive architectures designed for the two strategies is the size of the cryogenic hydrogen tank, which will be higher for the full hybrid mission design due to the higher quantity of hydrogen it needs to carry to cover the diversion and holding flight segments. As it can be seen in the graph on the right, the mass of hydrogen is almost doubled for the full hybrid mission. Although not particularly inconvenient in terms of added weight penalty, it is still seriously challenging in terms of volume. Moreover, the lower OWE for the main hybrid mission design also implies higher payload capabilities and therefore slightly better performances in terms of block fuel per passenger. For these reasons, it was decided to continue the analyses only using the main hybrid mission strategy.

Figure 26 shows the most relevant results of a second parametric study which was performed in order to evaluate the impact of the design range on the hybrid aircraft performance. Three design ranges have been considered for the study: $200NM$, $400NM$ and $600\ NM$. By varying the electrical power between $200\ kW$ and $800\ kW$, the block fuel

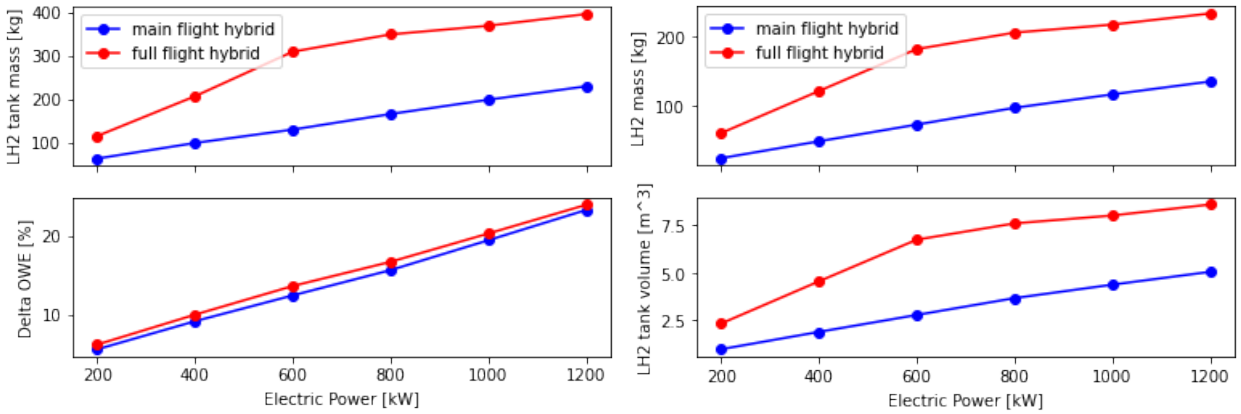

(a) LH_2 tank mass and delta OWE variation w.r.t. baseline **(b) LH_2 mass and tank volume variation**

Fig. 25 Main results of the parametric study for the selection of the hybridization strategy

per passenger appears to decrease almost linearly with the increase of the hybridization factor for all the three design ranges investigated. At 800 kW, there seems to be an optimum, after which the increase of H_p leads to a deterioration of the performances, again for all the three ranges. This optimum is given by a combination of two separate effects.

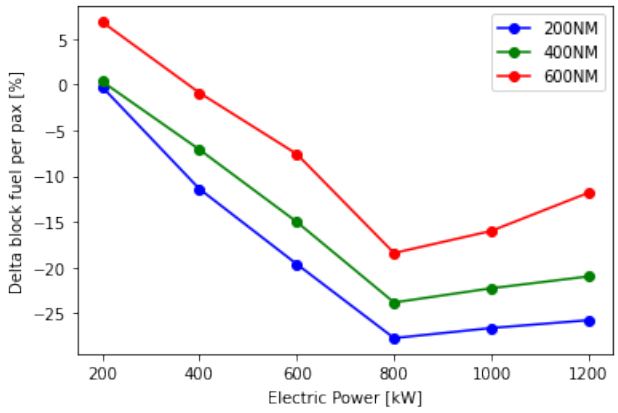

Fig. 26 Delta block fuel per pax variation for main flight hybrid w.r.t. baseline aircraft

First, at 800 kW of nominal electric power, according to the sizing criteria of the gas-turbine expressed at the beginning of this paragraph, the take-off power of the gas-turbine is about 1200 kW, which appears to be the minimum power required to allow the execution of the reserve flight mission without the aid of the electrical power. Therefore, for all the designs with a nominal electrical power above 800 kW, the increase of the H_p does not lead anymore to a consequent reduction in gas-turbine size, which thereby results in higher weight and fuel consumption.

The second effect is related to the variation of the specific energy of the hydrogen-based electric system with the increase of the H_p. With this term, the authors refer to the combination of all the equipment and the systems that are needed to generate and supply electrical power to the electric core and it includes: hydrogen mass, hydrogen tank, hydrogen distribution, fuel cell systems (as defined in Eq. (12)), and radiators for cooling. The specific energy is therefore calculated as follows:

$$E_{sp} = \frac{m_{H_2} \times FHV_{H2} \times \eta_{fc}}{m_{H_2} + m_{tank} + m_{distr} + m_{fc} + m_{radiators}} \tag{32}$$

The aforementioned definition of specific energy is particularly meaningful because it can be considered as the equivalent specific energy required by the batteries in order to have the same performance as the hydrogen-based system herein designed. Figure 27 shows the variation of the specific energy of the system related to the change of design range and

nominal electrical power. It can be seen, how for each range there seems to be an optimal point at which corresponds the highest specific energy, this point being the 800 kW for which the hybrid aircraft design showed the best performance in Fig. 26. This behaviour is given by the fact that most of the components of the system have masses that do not scale linearly with the electric sizing power, as shown in Fig. 9. The power-to-weight ratio of the fuel cell system increases rapidly till reaching an almost constant trend. Past this crucial point, increasing the electrical power leads to an increase of the radiators mass which already at 800 kW has become significantly high to be comparable to the fuel cell system mass (see Fig. 28: the radiator mass is referred to with the label "cooling").

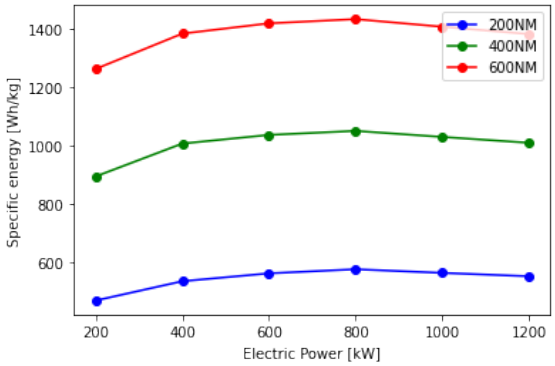

Fig. 27 Variation of system specific energy

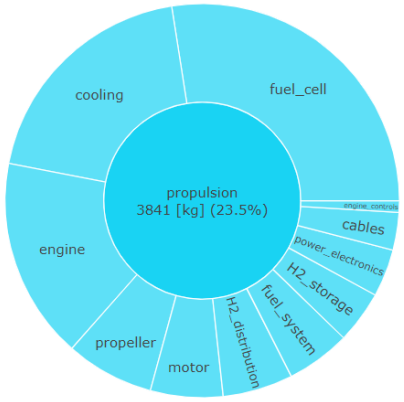

Fig. 28 Propulsion weight breakdown of the architecture designed for 200 NM and 800 kW

Furthermore, always from Fig. 9 it can be observed that there is an appreciable variation of the system specific energy with respect to the range variation. The increase in design range has only an impact on the hydrogen consumption, and consequently on the mass of the hydrogen tank, but it does not affect cooling requirements and fuel cell system size which are driven mainly by the nominal electric power of the system. Since the tank mass is a relatively small percentage of the entire hybrid propulsion system, the aforementioned behaviour is explained. Nevertheless, in terms of absolute values, the total mass of the propulsive system with a certain sizing electrical power is still higher with increasing design range, due to the bigger and heavier tanks. This added mass penalty results in a reduction of the max payload which translates in worse performance in terms of block fuel per passenger, as illustrated in Fig. 26. Considering also the volume constraints to integrate on the aircraft voluminous hydrogen tanks, the design range of 200 NM seems to be the most profitable and viable option. Therefore hereafter, additional analyses and considerations on the hybrid aircraft design are only given considering a design range of 200 NM. The main performance of hybrid aircraft configurations is summarized in Table 5.

A/C conf	$P_{elec}(P_{gt_{TO}})$	**TOW** kg	M_{cr}	PAX	**TT** min	kgH_2	$kgCO_{2eq}/PAX$	gNO_x/PAX
Baseline	0 (1.8) MW	22108	0.489	72	45.9	0	29.9	21.9
1:H_p=0.11	0.2 (1.6) MW	23020	0.442	72	50	24.5	30.7	21.5
2:H_p=0.22	0.4 (1.4) MW	23480	0.449	72	49.5	48.9	27.4	18.7
3:H_p=0.34	0.6 (1.2) MW	23573	0.457	69	48.9	72.9	25.1	16.4
4:H_p=0.45	0.8 (1.0) MW	23573	0.465	65	48.4	97	**22.8**	**13.9**
5:H_p=0.51	1.0 (1.0) MW	23573	0.486	59	46.1	116.3	23.3	13.1
6:H_p=0.56	1.2 (1.0) MW	23573	0.505	54	44.2	134.8	23.8	12.3

Table 5 Main aircraft performance for a mission of 200NM for six different hybridization factors

The table reports the results for a 200NM mission for the baseline aircraft and different hybrid aircraft configurations according to six different hybridization levels. It shows, among others, the aircraft performance in terms of emissions, hydrogen consumption and trip time, meaning the time required to perform the flight segments of climb, cruise and

descent without taking into account the ground operations. With the exception of the last hybrid configuration, which is characterized by an higher installed total power due to the minimal gas-turbine power requirement for the reserve flight, the time spent to carry out the flight is higher for the hybrid aircraft compared to the baseline aircraft due to the higher TOW which also affects the max cruise speed. However, the trip time decreases with increasing hybridization level. This happens because the electric power output is not affected by the change in altitude and Mach number, contrarily to the gas-turbine engine, therefore the total available power of the hybrid propulsion system at high altitude is greater for higher hybridization levels, despite having the same total take-off power. Concerning the emissions, for the first hybrid configuration the hybridization level is not sufficiently high to offset the mass penalty of the hybrid system with a significant reduction of fuel consumption. However for all the other configurations, regardless of the decrease of the allowed number of passengers, appreciable reduction of both CO_{2eq} and NO_x can be observed, with peaks for the fourth configuration of -24% and -40%, respectively.

VI. Conclusion

The scope of this study was to explore the potential of hybrid electric propulsion comprising hydrogen fuel cells for the regional aircraft class certified according to the CS-25. Starting from a baseline conventional turboprop aircraft designed using an overall aircraft design tool derived from $FAST\text{-}OAD$, an hybrid electric aircraft model was designed by replacing its propulsion system with hybrid electric fuel-cell based propulsion. Then, an MDA process was used to size the propulsion system according to the required design range and electric nominal power and to evaluate its performance with respect to the baseline conventional aircraft. This "forward-fit" approach was preferred to a dedicated ex-novo design, because the objective of the study was not to identify or to design the best possible hybrid aircraft configuration, but rather to provide a reliable preliminary assessment of the performance of the hydrogen fuel-cell based propulsion applied on a large turboprop passenger aircraft. In this way, the delta of the performance between the two aircraft is exclusively determined by the effectiveness of each propulsion system. Moreover, this approach allows getting rid of the uncertainties issued by the models that are not directly related to the propulsion. Parametric studies were conducted in order to understand the impact on the hybrid aircraft performance of design range and nominal electrical power of the system. The study showed that the lowest range of 200 NM is the most advantageous choice both in terms of emission reduction and ease of hydrogen tank integration. Concerning the variation of the nominal electric power of the system, the highest levels of emission reduction are reached with the configuration having an hybridization factor of 0.45, which corresponds to an electric power of 800 kW per side.

To conclude, the results obtained show that, while being much more complex than battery-based electric propulsion, the hydrogen-based electric propulsion has the potential to considerably reduce aircraft emissions even with today state-of-the-art technological levels. Moreover, considering that some of these technologies (e.g. electric motors, fuel cells) have seen a steep evolution and improvement curve in the past few years, thanks also to their application on serial production vehicles, higher benefits can still be expected for the next future. In addition to that, the hybrid fuel cell system was sized according to design variables which were only chosen based on some preliminary trade studies which do not necessarily guarantee the optimal results. A dedicated multidisciplinary optimization, which is envisaged for the future work of this research, would allow for a wider exploration of the design space of the hybrid propulsive system, potentially providing even better results. Nevertheless, many challenges still remain to be addressed which concern mainly safety requirements, space allocation of these voluminous systems on board an aircraft and their impact on the aircraft center of gravity, thus its stability and handling qualities. The thermal management of PEM fuel cells is a major challenge because of the low operating temperatures. The results showed that low-temperature PEM fuel cells require large and heavy radiators to evacuate the waste heat. However, a new technology of PEM fuel cells operating at higher temperatures (named HT-PEM) could allow to considerably reduce the weight penalties of the thermal management system. Increasing the fuel cell operating temperature would lead to higher heat recovery for the heating of the liquid hydrogen as well as a reduction of waste heat due to the higher heat required to keep the fuel cell at the nominal operational temperature. Finally, more advanced technologies for thermal management such as skin heat exchangers may be used rather than traditional ram air radiators. This technology exploits the heat sink potential of the aircraft surface to cool down the coolant fluid. Such technology is very promising both in terms of weight savings and reduced aerodynamics penalties, since it does not require the integration of ram air inlets. To the knowledge of the authors, skin heat exchangers have been developed and manufactured by Liebherr Aerospace who successfully tested the system on a A320 provided by the DLR institute in 2014 [49]. The technology readiness level (TRL) of both the HT-PEM technology and skin-heat exchangers is still not mature enough to have sufficient information to perform

reliable analyses, but their promising performance could be among the key enablers for the development of a fuel cell based hydrogen propulsion system in the future.

Appendix

This section shows the most relevant equations of the methods introduced in Section III used to size and to design the gas turbine as well as the cryogenic tank.

Gas turbine mass equations

$$m_{eng} = 0.758 \left(\frac{P_{gt}}{745.7} \right)^{0.803} \tag{33}$$

m_{eng} includes both gas turbine and gearbox masses. Units are in SI.

$$m_{nacelle} = 0.43 m_{eng} \tag{34}$$

$$m_{prop} = 0.5 \left(\frac{D_p P_{gt} \sqrt{B}}{227.2} \right)^{0.52} \tag{35}$$

$$m_{ps} = m_{ec} + m_{ess} + m_{osc} \tag{36}$$

$$m_{ec} = 0.454(5N_{eng} + 2.63 l_{fuselage}) \tag{37}$$

$$m_{ess} = 22.31 \left(\frac{m_{eng} N_{eng}}{453.59} \right)^{0.541} \tag{38}$$

$$m_{osc} = 0.07 m_{eng} \tag{39}$$

Cryogenic tank design equations

$$a = \left(\frac{3V_t \phi^2 (1-\lambda)}{\pi \psi (2\lambda + 4)} \right)^{1/3} \tag{40}$$

$$b = \psi c \tag{41}$$

$$c = \frac{a}{\phi} \tag{42}$$

$$l_s = \frac{V_t - (4/3)\pi abc}{\pi ac} \tag{43}$$

$$V_t = \frac{y m_{H_2}}{\rho_{LH_2}} + \frac{(1-y) m_{H_2}}{\rho_{GH_2}} \tag{44}$$

ρ_{LH_2} and ρ_{GH_2}= linear regression from [19].

$$\rho_{LH_2} = -0.019(p_{fill}^3) + 0.3287(p_{fill}^2) - 3.7129 p_{fill} + 73.424 \tag{45}$$

y = linear interpolation from [19].

$$\rho_{GH_2} = 1.4909 p_{fill} + 0.4182 \tag{46}$$

$$y = \alpha p_{fill} + y_0 \tag{47}$$

$$p_p = k_s(p_v - 1)10^5 \tag{48}$$ Safety factor k_s=1.5

Sphere

$$s_w = \frac{a p_p}{2K/S - p_p} \tag{49}$$

$$S_i = 4\pi a^2 \tag{50}$$

Ellipsoid with cylindrical shell

$$K/S \geq p_p \left[\frac{a+c}{2s_w} \left(1 + 2 \left(1 + 3.6 \frac{p_p}{E_Y} \left(\frac{a+c}{2s_w} \right)^3 \right) \frac{a-c}{a+c} \right) + 0.5 \right] \tag{51}$$

$$S_i = S_{ell} + S_{cyl} \tag{52}$$

$$S_{ell} = 4\pi \sqrt[1.6]{\frac{a^{1.6}b^{1.6} + a^{1.6}c^{1.6} + b^{1.6}c^{1.6}}{3}} \tag{53}$$

$$S_{cyl} = l_s \pi (3(a+c) - \sqrt{10ac + 3(a^2 + c^2)}) \tag{54}$$

$$m_{tank} = S_i(s_w \rho_w + s_{ins} \rho_{ins}) \tag{55}$$

Acknowledgments

This work is part of the activities of ONERA - ISAE - ENAC joint research group in a context of a partnership between ONERA, ISAE-SUPAERO and ATR. The authors would like to thank the group of students of ISAE-SUPAERO who worked on the modeling of the cryogenic tank design and in particular the student Felix Pollet who also worked on the modelling of the fuel cell balance of plant and thermal management. The authors would also like to thank ATR aircraft for the financial support of this research.

References

[1] Darecki, M., Edelstenne, C., Enders, T., Fernandez, E., Hartman, P., Herteman, J.-P., Kerkloh, M., King, I., Ky, P., Mathieu, M., et al., "Flightpath 2050 Europes Vision for Aviation," *Off. Eur*, 2011.

[2] Agarwal, R. K., "Review of technologies to achieve sustainable (green) aviation," *Recent advances in aircraft technology*, Vol. 19, 2012, pp. 427–464.

[3] ETN, "The path towards a zero-carbon gas turbine," `https://etn.global/wp-content/uploads/2020/01/ETN-Hydrogen-Gas-Turbines-report.pdf`, 2020.

[4] Brelje, B. J., and Martins, J. R. R. A., "Electric, hybrid, and turboelectric fixed-wing aircraft: A review of concepts, models, and design approaches," *Progress in Aerospace Sciences*, Vol. 104, 2019, pp. 1–19.

[5] Gesell, H., Wolters, F., and Plohr, M., "System analysis of turbo-electric and hybrid-electric propulsion systems on a regional aircraft," *The Aeronautical Journal*, Vol. 123, No. 1268, 2019, pp. 1602–1617.

[6] Zamboni, J., Vos, R., Emeneth, M., and Schneegans, A., "A method for the conceptual design of hybrid electric aircraft," *AIAA Scitech 2019 Forum*, 2019, p. 1587.

[7] Cameretti, M. C., Del Pizzo, A., Di Noia, L. P., Ferrara, M., and Pascarella, C., "Modeling and investigation of a turboprop hybrid electric propulsion system," *Aerospace*, Vol. 5, No. 4, 2018, p. 123.

[8] Finger, D. F., Braun, C., and Bil, C., "Comparative assessment of parallel-hybrid-electric propulsion systems for four different aircraft," *Journal of Aircraft*, 2020, pp. 1–11.

[9] Thauvin, J., "Exploring the design space for a hybrid-electric regional aircraft with multidisciplinary design optimisation methods," Ph.D. thesis, 2018.

[10] Company, M. ., "Hydrogen-powered aviation: A fact-based study of hydrogen technology, economics, and climate impact by 2050," 2020.

[11] Romeo, G., Borello, F., Correa, G., and Cestino, E., "ENFICA-FC: Design of transport aircraft powered by fuel cell & flight test of zero emission 2-seater aircraft powered by fuel cells fueled by hydrogen," *International journal of hydrogen energy*, Vol. 38, No. 1, 2013, pp. 469–479.

[12] Kallo, J., "DLR leads HY4 project for four-seater fuel cell aircraft," *Fuel Cells Bulletin*, Vol. 2015, No. 11, 2015, p. 13.

[13] Osborne, T., "Startup sees fuel cell future for regional aviation: ZeroAvia planning 300-mi. endurance flight in early 2020; hydrogen production facilities could be sited at airports and use renewable energy," *Aviation Week & Space Technology*, 2019.

[14] David, C., and Delbecq, S., "FAST-OAD: Future Aircraft Sizing Tool - Overall Aircraft Design," `https://fast-oad.readthedocs.io/`, 2020. Accessed: 2020-06-15.

[15] David, C., Delbecq, S., Defoort, S., Schmollgruber, P., Benard, E., and Pommier-Budinger, V., "From FAST to FAST-OAD: An open source framework for rapid Overall Aircraft Design," European Aeronautics Science Network, 2020.

[16] Lambe, A. B., and Martins, J. R., "Extensions to the design structure matrix for the description of multidisciplinary design, analysis, and optimization processes," *Structural and Multidisciplinary Optimization*, Vol. 46, No. 2, 2012, pp. 273–284.

[17] Sgueglia, A., "Methodology for sizing and optimising a Blended Wing-Body with distributed electric ducted fans," Ph.D. thesis, ISAE-Institut Supérieur de l'Aéronautique et de l'Espace, 2019.

[18] Raymer, D., *Aircraft design: a conceptual approach*, American Institute of Aeronautics and Astronautics, Inc., 2012.

[19] Winnefeld, C., Kadyk, T., Bensmann, B., Krewer, U., and Hanke-Rauschenbach, R., "Modelling and designing cryogenic hydrogen tanks for future aircraft applications," *Energies*, Vol. 11, No. 1, 2018, p. 105.

[20] Dupont, W. P., and Colongo, C., *Preliminary design of a commercial transport aircraft.*, Vol. 2nd ed. Class notes, ISAE-Supaero, 2012.

[21] Roskam, J., *Airplane design*, DARcorporation, 1985.

[22] Teeuwen, Y., "Propeller Design for Conceptual Turboprop Aircraft," Master's thesis, Delft University of Technology, 2017.

[23] Lenssen, R., "Series Hybrid Electric Aircraft: Comparing the Well-to-Propeller Efficiency with a Conventional Propeller Aircraft," Master's thesis, Delft University of Technology, 2016.

[24] Stückl, S., "Methods for the design and evaluation of future aircraft concepts utilizing electric propulsion systems," Ph.D. thesis, Technische Universität München, 2016.

[25] Vratny, P. C., "Conceptual design methods of electric power architectures for hybrid energy aircraft," Ph.D. thesis, Technische Universität München, 2019.

[26] Hoogendoorn, J., "Fuel Cell and Battery Hybrid System Optimization: Towards Increased Range and Endurance," Master's thesis, Delft University of Technology, 2018.

[27] Lototskyy, M. V., Tolj, I., Pickering, L., Sita, C., Barbir, F., and Yartys, V., "The use of metal hydrides in fuel cell applications," *Progress in Natural Science: Materials International*, Vol. 27, No. 1, 2017, pp. 3–20.

[28] GmbH, A. D., "Liquid Hydrogen Fuelled Aircraft – System Analysis," Final report GRD1-1999-10014, 2003.

[29] Cells, F., and Undertaking, H. J., "INN-BALANCE project," `https://www.innbalance-fch-project.eu/`, 2018. Accessed: 2020-11.

[30] AKG-Group, "AKG-Line A Oil-to-Air cooling systems with AC-motor," https://www.akg-group.com/fileadmin/user_upload/Brochures/AKG-Line/AKG_LineA_en.pdf, 2020. Accessed: 2020-11.

[31] Islam, M., Shabani, B., Rosengarten, G., and Andrews, J., "The potential of using nanofluids in PEM fuel cell cooling systems: A review," *Renewable and Sustainable Energy Reviews*, Vol. 48, 2015, pp. 523–539.

[32] Berger, O., "Thermodynamische Analyse eines Brennstoffzellensystems zum Antrieb von Kraftfahrzeugen," *Duisburg/Essen, Technische Universität, Dissertation*, 2009.

[33] Teichel, S., Dörbaum, M., Misir, O., Merkert, A., Mertens, A., Seume, J., and Ponick, B., "Design considerations for the components of electrically powered active high-lift systems in civil aircraft," *CEAS Aeronautical Journal*, Vol. 6, No. 1, 2015, pp. 49–67.

[34] Fumatech, "Membrane Humidifiers: fumasep High Performance Membrane Humidifiers for Fuel Cells," https://www.fumatech.com/NR/rdonlyres/0B9A1C7F-5BA6-4409-A003-5C4E79CD61AB/0/FUMATECH_BWT_GmbHMembrane_Humidifiers.pdf, 2020. Accessed: 2020-11.

[35] Larminie, J., Dicks, A., and McDonald, M. S., *Fuel cell systems explained*, Vol. 2, J. Wiley Chichester, UK, 2003.

[36] Verstraete, D., "The potential of liquid hydrogen for long range aircraft propulsion," Ph.D. thesis, Cranfield University, 2009.

[37] Capps, R. W., "Selecting the optimum pipe size," *Chemical Engineering*, Vol. 102, No. 7, 1995, p. 128.

[38] Mattingly, J. D., *Elements of gas turbine propulsion*, McGraw-Hill, 1996.

[39] Oates, G. C., *Aerothermodynamics of gas turbine and rocket propulsion*, American Institute of Aeronautics and Astronautics, 1997.

[40] Skellett, A., "National Advisory Committee for Aeronautics, Nineteenth Annual Report," ????

[41] PowerCell, "PowerCell S3 datasheet," https://www.powercell.se/wordpress/wp-content/uploads/2018/12/S3-Produktblad-190430.pdf, 2020. Accessed: 2020-11.

[42] Solomon, S., Qin, D., Manning, M., Chen, Z., Marquis, M., Averyt, K., Tignor, M., and Miller, H., "IPCC fourth assessment report (AR4)," *Climate change*, 2007.

[43] JRC, R. E., Hass, H., Larivé, J.-F., JRC, L. L., Maas, H., and Rickeard, D., "Well-to-wheels Report Version 4.a JEC Well-to-wheels analysis," *Institute for Energy and Transport, Joint Research Centre, Luxembourg: Publications Office of the European Union*, Vol. 2014, 2014.

[44] Guynn, M. D., *Evaluation of an aircraft concept with over-wing, hydrogen-fueled engines for reduced noise and emissions*, NASA Langley Research Center, 2002.

[45] Sherwood, S. C., Dixit, V., and Salomez, C., "The global warming potential of near-surface emitted water vapour," *Environmental Research Letters*, Vol. 13, No. 10, 2018, p. 104006.

[46] Marketing, A., "ATR72-600 booklet," https://www.skybrary.aero/bookshelf/books/3696.pdf, 2018. Accessed: 2021-06.

[47] Bowman, C. L., Felder, J. L., and Marien, T. V., "Turbo-and Hybrid-electrified aircraft propulsion concepts for commercial transport," *2018 AIAA/IEEE Electric Aircraft Technologies Symposium (EATS)*, IEEE, 2018, pp. 1–8.

[48] Ehsani, M., Gao, Y., Longo, S., and Ebrahimi, K., *Modern electric, hybrid electric, and fuel cell vehicles*, CRC press, 2018.

[49] Pagnano, G., "Overview of Clean Sky Technical Programme And Achievements to date," https://www.cleansky.eu/sites/default/files/documents/Giuseppe%20Pagnano%20Presentation%20Aerodays.pdf, 2015. Accessed: 2021-06-14.